Available online at www.sciencedirect.com
SCIENCE DIRECT®
Journal of Sound and Vibration 285 (2005) 803–834
JOURNAL OF SOUND AND VIBRATION
www.elsevier.com/locate/jsvi

Super-harmonics in a torsional system with dry friction path subject to harmonic excitation under a mean torque

Chengwu Duan, Rajendra Singh*

Acoustics and Dynamics Laboratory, Department of Mechanical Engineering, The Center for Automotive Research, The Ohio State University, 650 Ackerman Road, Columbus, OH 43210, USA

Received 16 February 2004; received in revised form 16 August 2004; accepted 30 August 2004
Available online 15 December 2004

Abstract

The nonlinear frequency response characteristics of a two-degree-of-freedom torsional system with a significant dry friction controlled path are studied, when excited by sinusoidal torque under a mean load. An analytical solution is first developed for a simplified system subjected to continuous slipping motions. The nature of super-harmonic peaks as generated by the dry friction nonlinearity is efficiently found. The effect of a non-zero mean load is also determined and qualitatively understood. Further, a refined multi-term harmonic balance method (MHBM) is proposed that includes up to 12 terms. It is used to study an automotive drive train system that experiences significant stick–slip motions. Associated computational issues including the selection of initial conditions are addressed. Studies show that the mean load could induce asymmetric stick–slip motions and accordingly it has significant effect on time and frequency domain responses. Reasons for the occurrence of super-harmonic resonant peaks and transitional peaks are investigated. Finally, our MHBM is applied to the conventional single-degree-of-freedom system where the spring path exists in parallel with a dry friction damper (Den Hartog's problem). Our predictions match well with Den Hartog's analytical solution. Den Hartog's system differs, in terms of the dynamic behavior, from our torsional system (with a sole dry friction path).

1. Introduction

Dry friction elements are commonly found in mechanical systems and yet much of prior research has focused on the dry friction damper and its characterization [1–6]. Den Hartog [1]

*Corresponding author. Tel.: +1 614 292 9044; fax: +1 614 292 3163.
E-mail address: singh.3@osu.edu (R. Singh).

0022-460X/$ - see front matter © 2004 Elsevier Ltd. All rights reserved.
doi:10.1016/j.jsv.2004.08.020

Nomenclature

C	torsional viscous damping coefficient
D	differential operator matrix
f	function
I	torsional inertia
H	characteristic matrix
J	Jacobian matrix
K	torsional stiffness
P	period
R	residue vector
t	time (dimensional)
T	torque

Greek letters

δ	relative angular displacement
ε	tolerance
ζ	viscous damping ratio
θ	absolute angular displacement
μ	friction coefficient
σ	conditioning factor
τ	dimensionless time
ϕ	phase angle
ψ	phase lag
Ω	excitation frequency (dimensionless)
ω	excitation frequency (rad/s)
Δ	discrete Fourier transform matrix

Subscripts

1,2,3	inertial element indices
e	engine
f	friction
k	kinetic
m	mean
max	maximum
min	minimum
n	natural frequency
p	fluctuating component or perturbation
s	static
sf	saturation

Superscripts

$\bar{}$	dimensional value
$\dot{}$	first derivative with respect to time
$\ddot{}$	second derivative with respect to time
$'$	first derivative with respect to dimensionless time
$''$	second derivative with respect to dimensionless time
-1	inverse
$+$	pseudo-inverse
T	transpose

Operators

$\|\ \|$	absolute value
$\|\|\ \|\|$	Euclidean or L_2 norm
$\langle\rangle_t$	time-average operator

Abbreviations

max	maximum value
min	minimum value
rms	root-mean-square value
DFT	discrete Fourier transform
MHBM	multi-term harmonic balance method
HBM	one-term harmonic balance method
sdof	single-degree-of-freedom system
TCC	torque converter clutch
2dof	two-degree-of-freedom system

initiated work in this area by analytically determining the forced harmonic response of a single-degree-of-freedom (sdof) system with combined Coulomb and viscous friction elements. But his solution was limited to no more than two stops. Pratt and Williams [2] extended Den Hartog's work and calculated the system response with multiple lock-ups by using a numerical shooting method. Wang [3] developed an analytical solution for the periodic response of a bi-linear hysteresis friction system. However, numerical iterations were still needed to match the solutions obtained from stick and slip states. Further, Menq and Yang [4], and Wang and Chen [5] have

used multi-term harmonic balance methods (MHBM) to find the dynamic response of a bi-linear hysteresis problem. Overall, three common features exist among the formulations that have been employed by many researchers [1–6]. First, only the primary harmonic resonances are examined under sinusoidal excitation. Second, a spring path is placed in parallel with the dry friction element, thus having two parallel paths for force transmission. Third, the saturation friction force is assumed to be small; this is obviously valid from the friction damper standpoint.

In our study we examine the dry friction element in those situations where it is a key path in transmitting mechanical power in real-life torsional systems rather than acting as a pure friction damper. For example, the controlled slip clutch technology is now being widely used in automotive drive train systems to increase fuel efficiency and to improve ride quality [7–10]. Clutch systems such as the automotive torque converter clutch (TCC) [7], smart clutch [8] and dual clutch transmission [9,10] employ the dry friction element as the sole or dominant power transmission path. The spring element is usually in series (but not in parallel) with the dry friction element. The scientific literature on such torsional problems is sparse. Recently, Duan and Singh [11] studied the TCC sub-system using numerical methods and constructed the nonlinear frequency responses based on the cyclic time histories under sinusoidal excitations in the presence of mean torques. However, a thorough understanding of the nonlinear characteristics is yet to be achieved. For instance, the existence of super-harmonics has not been demonstrated, especially when a mean torque load is also applied. This article will focus on the above-mentioned issues and propose semi-analytical methods for a two-degree-of-freedom (2dof) torsional system with a single dry friction element of relatively high saturation torque.

2. Problem formulation

2.1. Physical system and governing equations

The 2dof definite torsional system of Fig. 1 represents, in a generic sense, key features of the automotive clutch systems [7,8,11]. The dry friction T_{f12} is the sole path that transmits torque from the flywheel to the downstream driveline system. Here, $\bar{I}_1$ represents the combined torsional inertia of flywheel, front cover and impeller, $\bar{I}_2$ is the inertia of friction shoe, and $\bar{I}_3$ is the lumped inertia of transmission, differential and vehicle. Further, $\bar{I}_3$ is reasonably approximated as a grounded inertia since it is substantial compared to $\bar{I}_1$ and $\bar{I}_2$ during the typical TCC operation, i.e. in a high gear position [7,12]. The governing equations for this 2dof torsional system are

$$\bar{I}_1\ddot{\bar{\theta}}_1 + \bar{T}_{f12}(t) = \bar{T}_e(\bar{t}) = \bar{T}_m + \bar{T}_p \sin(\bar{\omega}\bar{t}), \tag{1a}$$

$$\bar{I}_2\ddot{\bar{\theta}}_2 + \bar{C}_{23}\dot{\bar{\theta}}_2 + \bar{K}_{23}\bar{\theta}_2 = \bar{T}_{f12}(t). \tag{1b}$$

Here, $\bar{\theta}_1$ and $\bar{\theta}_2$ are the absolute angular displacements, $\bar{C}_{23}$ is the lumped viscous damping between the friction shoe and the rest of the driveline, $\bar{K}_{23}$ is the linear torsional stiffness, and

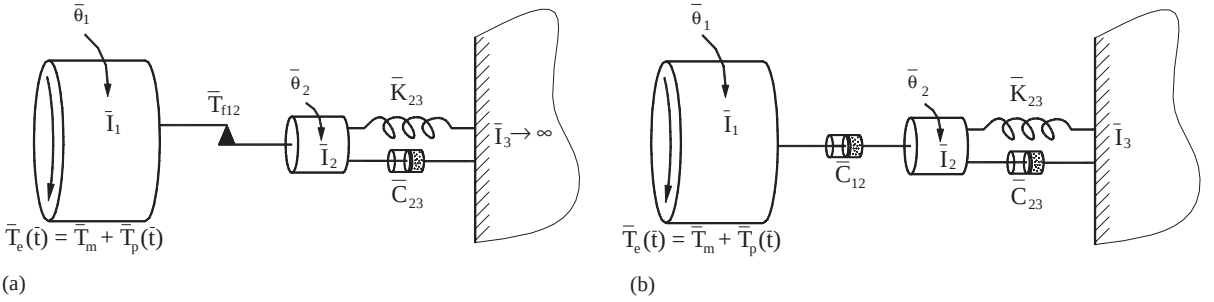

Fig. 1. Schematic of the 2dof torsional automotive dry friction clutch system. (a) Nonlinear model, (b) linear system with viscous damper. All parameters and variables have dimensions.

$\bar{T}_e(\bar{t})$ is the engine torque excitation composed of mean torque $\bar{T}_m = \langle \bar{T}_e \rangle_{\bar{t}}$ and pulsating $\bar{T}_p(\bar{t})$ components; here $\langle\rangle_{\bar{t}}$ is the time-average operator. The pulsating torque generally contains many harmonic (or torque order) components. However, in this study we will only consider one term, i.e. $\bar{T}_e(\bar{t}) = \bar{T}_m + \bar{T}_p \sin(\bar{\omega}\bar{t})$, where $\bar{\omega} = (N_e/2)\bar{\Omega}_e$ is the dominant frequency for a multi-cylinder engine [13]; here, N_e is the number of engine cylinders and $\bar{\Omega}_e$ is the engine speed.

In Eq. (1), $\bar{T}_{f12}(t) = \bar{T}_{\rm sf} f(\dot{\bar{\theta}}_1 - \dot{\bar{\theta}}_2)$ is the nonlinear friction torque, which is a function (f) of the relative velocity $\dot{\bar{\theta}}_1 - \dot{\bar{\theta}}_2$ across the friction interface, and $\bar{T}_{\rm sf}$ represents the saturation friction torque. Further, the classic Coulomb model is used and static and kinetic friction coefficients are assumed to be the same. The normal force on the friction interface remains unchanged and the friction torque $\bar{T}_{\rm sf}$ is accordingly constant during the slip state.

The governing equations (1a,b) are then non-dimensionalized for three reasons. First, this process would reduce the number of system parameters and would permit more efficient parametric studies. Second, the numerical integration (or iteration) procedure is easier with a dimensionless formulation. Finally, the resulting dimensionless frequency would help in mapping the nonlinear frequency response characteristics. The dimensionless parameters are given as follows; also refer to Nomenclature for identification.

$$\bar{\omega}_n = \sqrt{\frac{\bar{K}_{23}}{\bar{I}_2}}, \quad I_1 = \frac{\bar{I}_1}{\bar{I}_2}, \quad I_2 = \frac{\bar{I}_2}{\bar{I}_2} = 1.0, \quad \zeta = \frac{\bar{C}_{23}}{2\sqrt{\bar{K}_{23}\bar{I}_2}}, \tag{2a–d}$$

$$T_m = \frac{\bar{T}_m}{\bar{T}_{\rm sf}}, \quad T_p = \frac{\bar{T}_p}{\bar{T}_{\rm sf}}, \quad \theta_1 = \frac{\bar{\theta}_1 \bar{K}_{23}}{\bar{T}_{\rm sf}}, \quad \theta_2 = \frac{\bar{\theta}_2 \bar{K}_{23}}{\bar{T}_{\rm sf}}, \tag{2e–h}$$

$$\Omega = \frac{\bar{\omega}}{\bar{\omega}_n}, \quad \tau = \bar{\omega}_n \bar{t}. \tag{2i,j}$$

Thus, the governing equations in dimensionless form are as follows where derivatives (superscripts $'$ and $''$) are with respect to dimensionless time τ:

$$I_1\theta_1'' + f(\theta_1' - \theta_2') = T_m + T_p \sin(\Omega\tau), \tag{3a}$$

$$\theta_2'' + 2\zeta\theta_2' + \theta_2 = f(\theta_1' - \theta_2'). \tag{3b}$$

For the case where relative motions are of interest, define $\delta_1(\tau) = \theta_1 - \theta_2$ and $\delta_2(\tau) = \theta_2 - \theta_3 = \theta_2$ since $\theta_3 = 0$ and rewrite the governing equations as

$$I_1\delta_1'' - 2\zeta I_1\delta_2' - I_1\delta_2 + (1 + I_1)f(\delta_1') = T_m + T_p \sin(\Omega\tau), \tag{4a}$$

$$\delta_2'' + 2\zeta\delta_2' + \delta_2 = f(\delta_1'). \tag{4b}$$

2.2. Objectives

The first major objective is to develop semi-analytical methods and determine the harmonic and super-harmonic responses of the torsional system of Fig. 1(a) and as described by Eq. (4). For the sake of illustration and validation, we will also apply our method to the sdof of Fig. 2 that has been used by many researchers [1,2,14]. For instance, Den Hartog obtained a closed-form solution under sinusoidal excitation by assuming non-stop frictional oscillations [1]. In this article, we will extend his study to a system with a single dry friction path and subject it to a sinusoidal excitation in the presence of a mean load. By obtaining a closed-form solution to this simplified system, better qualitative understanding of the nonlinear characteristics could be obtained. Further, in those cases where multiple-stops take place, time domain integration methods are usually employed [2,6]. However, the solution process is time-intensive since the numerical integration step has to be very small to capture the stick–slip transitions. Also, it takes significant time to obtain a steady-state response, especially for a lightly damped system. Some researchers [5,14] also utilized the incremental harmonic balance methods (IHBM) to examine the friction damper that was placed in parallel with spring elements. However, their methods are generally limited to three harmonics. This is not sufficient for our system since significant stick–slip motions could take place. Accordingly, in this article, a refined multi-term harmonic balance method (MHBM) that can accommodate up to 12 harmonics is proposed to predict the nonlinear characteristics in a more efficient way.

The second major objective is to generate the nonlinear frequency response characteristics of a torsional system with a dry friction controlled path and in particular to demonstrate the existence of super-harmonic resonances. Much of the prior work on dry friction damper system (as in Fig. 2) is limited to an examination of response in the vicinity of primary harmonic resonance [4,5,14]. However, we intend to show that significant super-harmonic resonances could exist in the system of Fig. 1(a). They are also controlled by the mean torque load and they could even dominate the time domain responses. To clearly show the super-harmonic resonances, the nonlinear frequency response maps will be constructed from the calculated steady-state cyclic time histories. Two kinds of frequency domain maps are presented in the subsequent sections. The first is the max–min map that is generated by picking the maximum (max) and minimum (min) response amplitudes at the excitation frequency (Ω) of interest; the second is the root-mean-square (rms) map by calculating the rms values of time history at each frequency. Also, the mean (dc term) values are plotted over the Ω range.

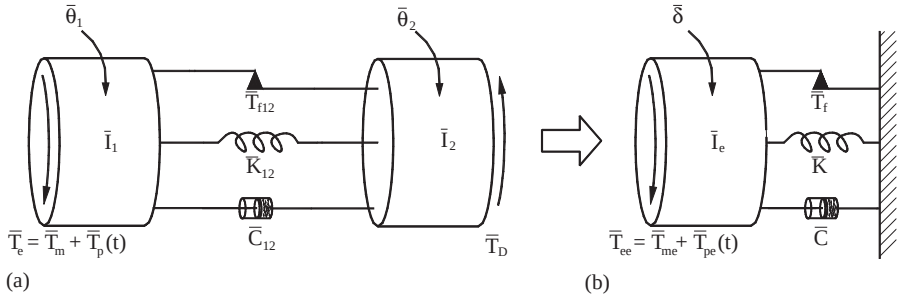

Fig. 2. Conventional friction damper system. (a) 2dof semi-definite system, (b) sdof definite system (Den Hartog's model [1]). All parameters and variables have dimensions.

3. Linear system analysis

For an automotive driveline coupled with a clutch, the whole system as in Fig. 1(a) may be modeled as a linear system under two premises: (1) assume the pure stick condition or (2) replace the dry friction element by a linear viscous damper. However, under the first premise, with a change in the inertia (for example, from I_2 to $I_1 + I_2$) and in the degree of freedom, the essential system properties such as natural frequencies and modes of the downstream sub-system will significantly change. Thus it is not suitable for benchmark studies. Consequently, in this section, we will analyze a linear system coupled by a viscous damper as shown in Fig. 1(b) using the second premise. The governing equations are obtained by replacing $f(\theta_1' - \theta_2')$ in Eq. (4) with $2\zeta_1(\theta_1' - \theta_2')$ where $\zeta_1 = \bar{C}_{12}/\left(2\sqrt{\overline{KI}_2}\right)$:

$$I_1\delta_1'' + (1 + I_1)2\zeta_1\delta_1' - 2\zeta I_1\delta_2' - I_1\delta_2 = T_m + T_p \sin(\Omega\tau), \tag{5a}$$

$$\delta_2'' + 2\zeta\delta_2' + \delta_2 = 2\zeta_1\delta_1'. \tag{5b}$$

A closer look at the above equations reveals that there has to be a mean velocity for δ_1' to balance the mean torque T_m under the dynamic condition. Further, T_m will be carried on to δ_2 through the viscous coupling. By assuming harmonic solutions, the mean part can be very easily obtained where $\langle\rangle_r$ implies time-average:

$$\langle\delta_1'(\tau)\rangle_\tau = T_m/2\zeta_1, \quad \langle\delta_2(\tau)\rangle_\tau = T_m. \tag{6a,b}$$

Note that these values remain constant as Ω changes. One could obtain complete analytical solutions for $\delta_1'(\tau)$and but the resulting expressions would be tediously long. Thus these are not included here. Rather, solutions are conveniently obtained by using a conventional numerical integration scheme such as Runge–Kutta. Sample frequency responses are presented in Fig. 3. It is seen that the relative velocity maintains an almost constant level except around $\Omega = 1.0$. As evident from Fig. 3(b), only the primary harmonic resonance appears in δ_2 as it should for a linear system. Numerical solutions confirm the analytical mean velocity $\langle\delta_1'(\tau)\rangle_\tau$ and mean displacement $\langle\delta_2(\tau)\rangle_\tau$ as observed in Fig. 3.

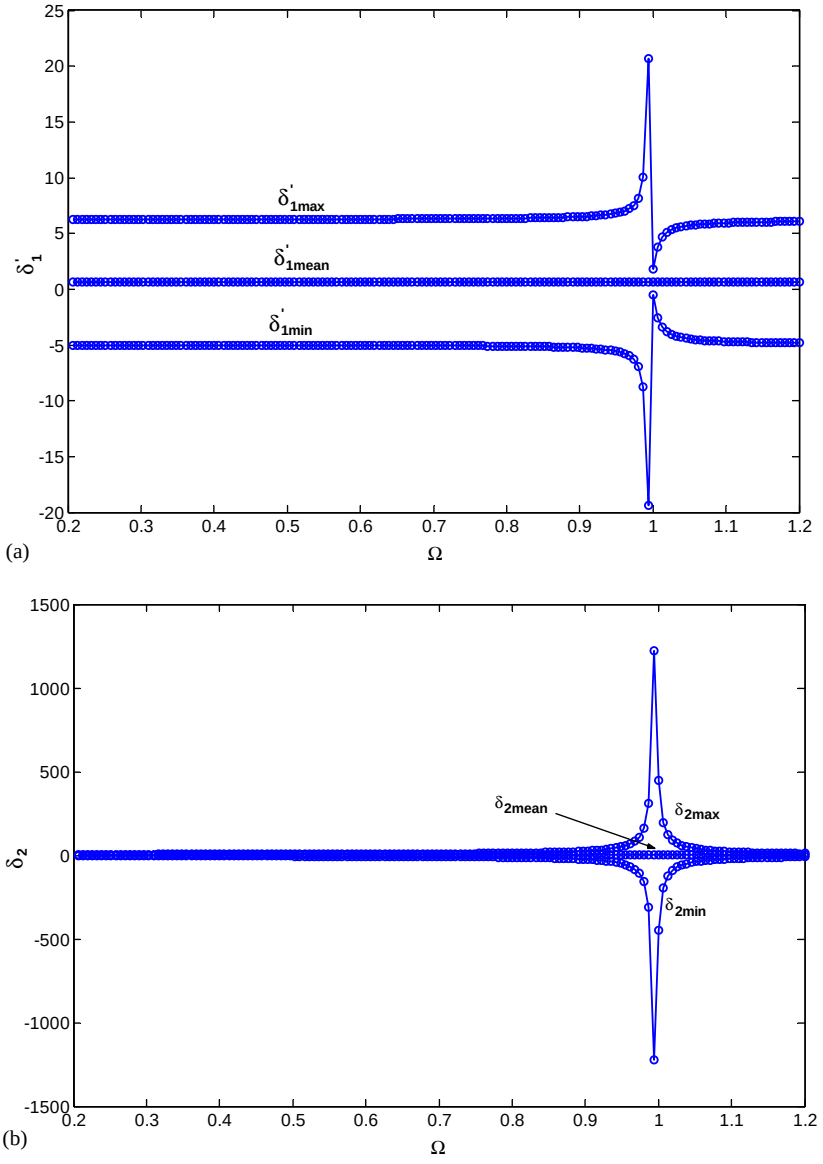

Fig. 3. Linear system frequency response for $I_1 = 0.01,\ \zeta_1 = 0.4,\ \zeta = 0.001,\ T_m = 0.5,\ T_p = 4.5$. (a) Max-mean-min frequency responses of δ_1', (b) max–min frequency response of δ_2.

4. Analytical solution using one-term harmonic balance method (HBM)

4.1. Closed-form solution to a simplified torsional system

First, an approximate analytical solution based on HBM is constructed for a simplified system to qualitatively establish the nature of nonlinear frequency responses and super-harmonic

resonances. In this simplified system (of Fig. 1(a)) we assume that $I_1 \ll 1.0$ and continuous slipping motion takes place across the friction interface. Further, $\delta_2 \ll \delta_1$ and $\delta_2' \ll \delta_1'$ are assumed. These assumptions are reasonable because the displacement and velocity of I_2 are constrained by the torsional spring and the viscous damper, respectively. Conversely, the dry frictional path, unlike the viscous damper which can at least constrain the velocity, cannot limit motions of I_1 especially in the presence of T_m. Thus, we further approximate Eq. (4) as

$$I_1\delta_1'' + f(\delta_1') = T_m + T_p \sin(\Omega\tau), \tag{7a}$$

$$\delta_2'' + 2\zeta\delta_2' + \delta_2 = f(\delta_1'). \tag{7b}$$

The above formulation essentially de-couples the 2dof definite system into two sdof sub-systems as shown in Figs. 4(a) and (b), respectively. Next, consider the system of Fig. 4(a) and Eq. (7a). The relative velocity and acceleration across the frictional interface, under harmonic excitation, are assumed as follows where the mean velocity A is a consequence of T_m, B is the amplitude of dynamic velocity and ϕ is the phase lag:

$$\delta_1' = A + B\sin(\Omega\tau + \phi), \quad \delta_1'' = B\Omega\cos(\Omega\tau + \phi). \tag{8a,b}$$

Assume profiles for relative velocity and corresponding friction torque as illustrated in Fig. 5. Note that an asymmetric slip motion occurs due to the mean velocity and the corresponding friction torque. i.e. $\delta'(\tau) \neq -\delta'(\tau + P/2)$ and $T_f(\tau) \neq -T_f(\tau + P/2)$, where $P = 2\pi/\Omega$ is the period. For continuous slipping motions, different amplitudes corresponding to positive or negative slip result due to the bias term A. However, in the case of stick–slip as explored in the subsequent section, the asymmetry could be introduced by either a bias term or even order harmonics. The transition times τ_1 and τ_2 (when T_f undergoes an abrupt change) can be determined by setting $\delta_1' = 0$ as

$$\Omega\tau_1 + \phi = -\sin^{-1}\frac{A}{B}, \quad \tau_1 = \frac{-\sin^{-1}A/B - \phi}{\Omega}, \tag{9a,b}$$

$$\Omega\tau_2 + \phi = \pi + \sin^{-1}\frac{A}{B}, \quad \tau_2 = \frac{\pi + \sin^{-1}A/B - \phi}{\Omega}. \tag{10a,b}$$

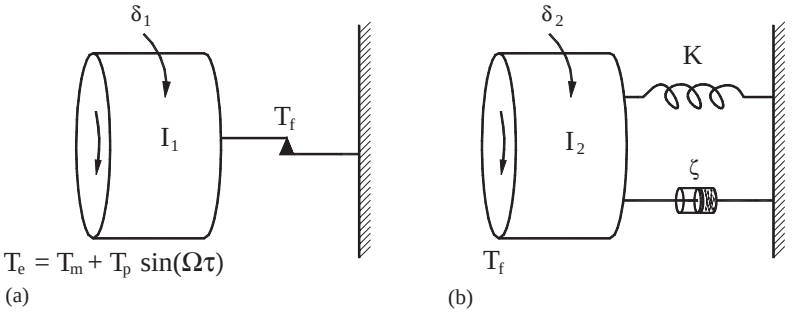

Fig. 4. Simplifications to Fig. 1(a) yield two de-coupled sub-systems. (a) Nonlinear sub-system with dry friction, (b) linear sub-system. Dimensionless parameters and variables are shown here.

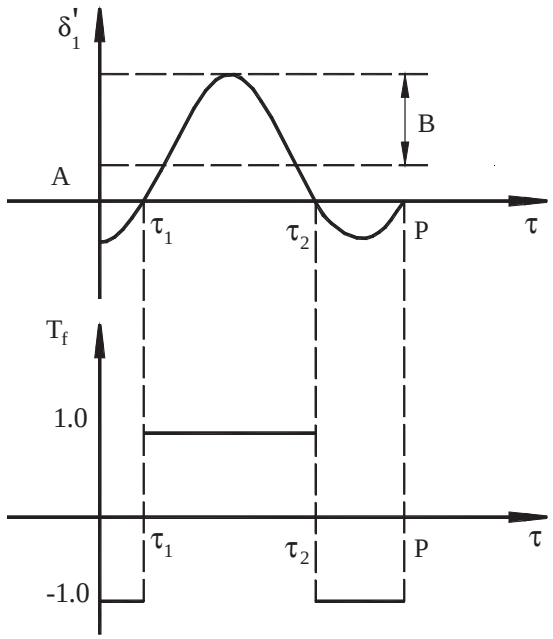

Fig. 5. Assumed time domain profiles for relative velocity and friction torque.

The corresponding friction torque is seen as follows:

$$T_f(\tau) = \begin{cases} 1.0, & \tau_1 \leqslant \tau < \tau_2, \\ -1.0, & \tau_2 \leqslant \tau < P + \tau_1. \end{cases} \tag{11}$$

Approximate the above expression using a truncated Fourier series as

$$T_f(\tau) = \frac{T_{f0}}{2} + \sum_{n=1}^{N} T_{cn} \cos(n\Omega\tau) + T_{sn} \sin(n\Omega\tau), \tag{12a}$$

$$T_{f0} = \frac{2}{P}\int_{\tau_1}^{P+\tau_1} T_f(\tau)\,\mathrm{d}\tau = \frac{\Omega}{\pi}\left(\tau_2 - \tau_1 - \frac{\pi}{\Omega}\right), \tag{12b}$$

$$T_{cn} = \frac{2}{P}\int_{\tau_1}^{P+\tau_1} T_f(\tau)\cos(n\Omega\tau)\,\mathrm{d}\tau = \frac{2}{n\pi}[\sin(n\Omega\tau_2) - \sin(n\Omega\tau_1)], \tag{12c}$$

$$T_{sn} = \frac{2}{P}\int_{\tau_1}^{P+\tau_1} T_f(\tau)\sin(n\Omega\tau)\,\mathrm{d}\tau = \frac{-2}{n\pi}[\cos(n\Omega\tau_2) - \cos(n\Omega\tau_1)]. \tag{12d}$$

Substituting T_{f0}, T_{c1} and T_{s1} into Eq. (7a) and applying the harmonic balance to both sides, we find the following nonlinear algebraic equations by sorting the like terms:

$$\frac{\Omega}{\pi}\left(\tau_2 - \tau_1 - \frac{\pi}{\Omega}\right) = T_m, \tag{13a}$$

$$I_1 B\Omega \cos(\phi) + \frac{2}{\pi}[\sin(\Omega\tau_2) - \sin(\Omega\tau_1)] = 0, \tag{13b}$$

$$-I_1 B\Omega \sin(\phi) - \frac{2}{\pi}[\cos(\Omega\tau_2) - \cos(\Omega\tau_1)] = T_p. \tag{13c}$$

Further, insert Eqs. (9b) and (10b) into Eq. (13a) to find

$$\sin^{-1}\frac{A}{B} = \frac{T_m\pi}{2}. \tag{14}$$

Since $\sin^{-1}(A/B)$ is bounded in $[-0.5\pi\ 0.5\pi]$, it is noted that $-1 \leqslant T_m \leqslant 1$. Analytically, if T_m is beyond such bounds, then either pure positive slip ($T_m > 1$) or pure negative slip ($T_m < -1$) motion takes place. In either case, the transmitted frictional torque $f(\delta_1')$ will always assume a constant value (± 1) accordingly. That would result in a constant relative displacement δ_2. Use trigonometric relations to observe the following:

$$\sin(\Omega\tau_2) - \sin(\Omega\tau_1) = 2\cos\left(\frac{T_m\pi}{2}\right)\sin(\phi), \tag{15a}$$

$$\cos(\Omega\tau_2) - \cos(\Omega\tau_1) = -2\cos\left(\frac{T_m\pi}{2}\right)\cos(\phi). \tag{15b}$$

Substitute Eq. (15) into Eqs. (13b) and (13c), respectively, and further simplify the nonlinear algebraic equations as

$$I_1 B\Omega \cos(\phi) + \frac{4}{\pi}\cos\frac{T_m\pi}{2}\sin(\phi) = 0, \tag{16a}$$

$$-I_1 B\Omega \sin(\phi) + \frac{4}{\pi}\cos\frac{T_m\pi}{2}\cos(\phi) = T_p. \tag{16b}$$

Finally, the closed-form solutions of A, B and ϕ of Eq. (8), corresponding to Fig. 4(a), can be obtained as

$$A = B\sin\frac{T_m\pi}{2}, \quad B = \frac{\sqrt{T_p^2\pi^2 - 16\cos^2(T_m\pi/2)}}{I_1\pi\Omega}, \tag{17a,b}$$

$$\phi = -\sin^{-1}\frac{\sqrt{T_p^2\pi^2 - 16\cos^2(T_m\pi/2)}}{T_p\pi}. \tag{17c}$$

Although A and B change with Ω, ϕ retains a constant value that is solely determined by the T_m and T_p. This is different from the first-order linear time-invariant system for which the ϕ varies with Ω [15]. Also, it differs from the classical dry friction damper system where a discontinuous jump in ϕ is seen at the primary resonance [1].

Once $\delta_1'(\tau)$ is obtained, the corresponding $T_f(\tau)$ is also determined, which now acts as an exciter for the sub-system 2 of Fig. 4(b). Feeding the solution of $T_f(\tau)$ into Eq. (7b), an analytical

solution for $\delta_2(\tau)$ is obtained:

$$\delta_2(\tau) = T_m + \sum_{n=1}^{N} \left\{ \frac{T_{cn}}{\Lambda_n} \cos(n\Omega\tau + \psi_n) + \frac{T_{sn}}{\Lambda_n} \sin(n\Omega\tau + \psi_n) \right\}, \tag{18a}$$

$$\Lambda_n = \sqrt{(1 - n^2\Omega^2)^2 + (2n\zeta\Omega)^2}, \quad \psi_n = -\tan^{-1} \frac{2n\zeta\Omega}{1 - n^2\Omega^2}. \tag{18b,c}$$

4.2. Analytical and numerical solutions

The analytical solutions obtained in previous section clearly reveal multiple harmonics in steady-state response of $\delta_2(\tau)$ and thereby raise the possibility of super-harmonic resonances. Typical analytical results in both time and frequency domains are shown in Figs. 6 and 7. These are compared with numerical solutions from a standard Runge–Kutta fifth (fourth)-order integration scheme with step size adaptation due to Dormand and Prince [16]. Excellent match between analytical and numerical solutions is achieved. Minor differences in the frequency response of velocity δ_1' are noticed at $\Omega = 1.0$ and 0.5. This is because the analytical solution does not account for a coupling between the sub-systems that is maximized at primary and super-harmonic resonances. And, differences in time domain velocity δ_1' result seem to produce minimal effects in the frequency response maps of δ_2 as seen in Fig. 7(b). Unlike the response for a linear system as observed in Fig. 3(b), super-harmonic resonances are generated in Fig. 7(b) by the dry friction nonlinearity at $\Omega = \frac{1}{3}$ and $\frac{1}{2}$, respectively.

Although the proposed analytical solution is limited to a simplified system with pure (or almost pure) slipping motion, the influence of T_m can be easily identified. From Eq. (17b), it is seen that the mean velocity A vanishes as T_m goes to zero. In this case, the friction interface would experience symmetric positive and negative slipping motions. These in turn would generate a symmetric square profile of the friction torque in Fig. 5. Thus, only the odd orders (1/3, 1/5, …) of T_f are generated and consequently only the odd-order super-harmonic resonances would occur in the response δ_2. Additionally, Fig. 8 shows that even a very small T_m will generate even orders (such as 1/2 and 1/4). For example, the 1/2 super-harmonic resonance is clearly observed in Fig. 8 at $\Omega = 0.5$ when $T_m = 0.2$.

4.3. Limitations

The HBM has been successful in qualitatively establishing the nature of super-harmonic resonances. Although the approximate analytical solution quickly predicts responses, it is valid only for a very simplified problem. In a more realistic driveline system, ignificant stick–slip motions occur and the assumption of continuous slipping motions is no longer valid. Thus, the analytical solution cannot provide accurate results for the system of Fig. 1(a), as evident from Fig. 9 for frequency responses and from Fig. 10 for corresponding time histories. For this reason, a refined MHBM is proposed in the next section to reasonably approximate the steady-state stick–slip motions under harmonic torque excitation given a mean load.

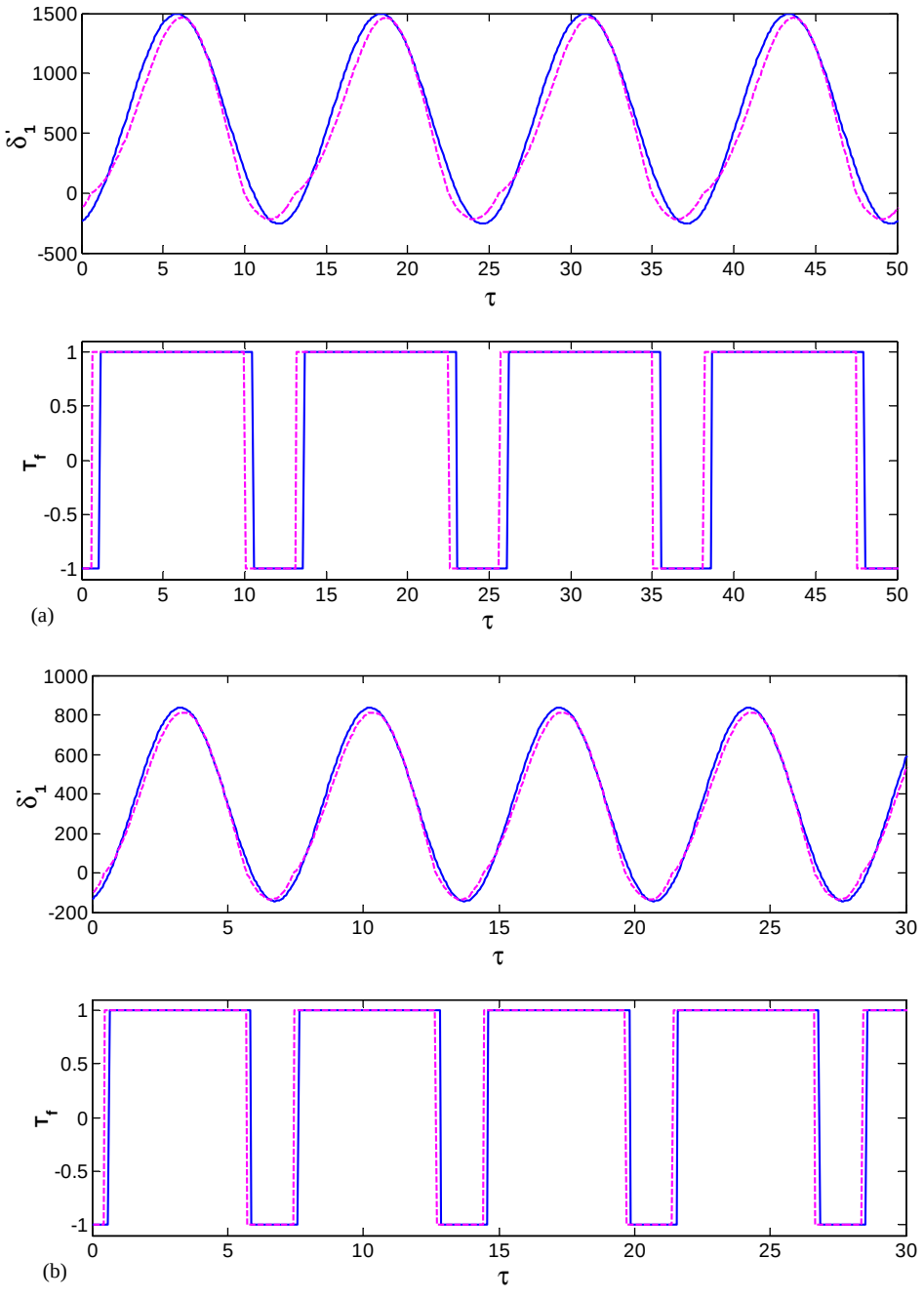

Fig. 6. Time histories for system of Fig. 4. Given $I_1 = 0.01$, $\zeta = 0.001$, $T_m = 0.5$, $T_p = 4.5$. (a) δ_1' and T_f at $\Omega = 0.5$: —, analytical solution; - - -, numerical solution. (b) δ_1' and T_f at $\Omega = 0.9$: —, analytical solution; - - -, numerical solution.

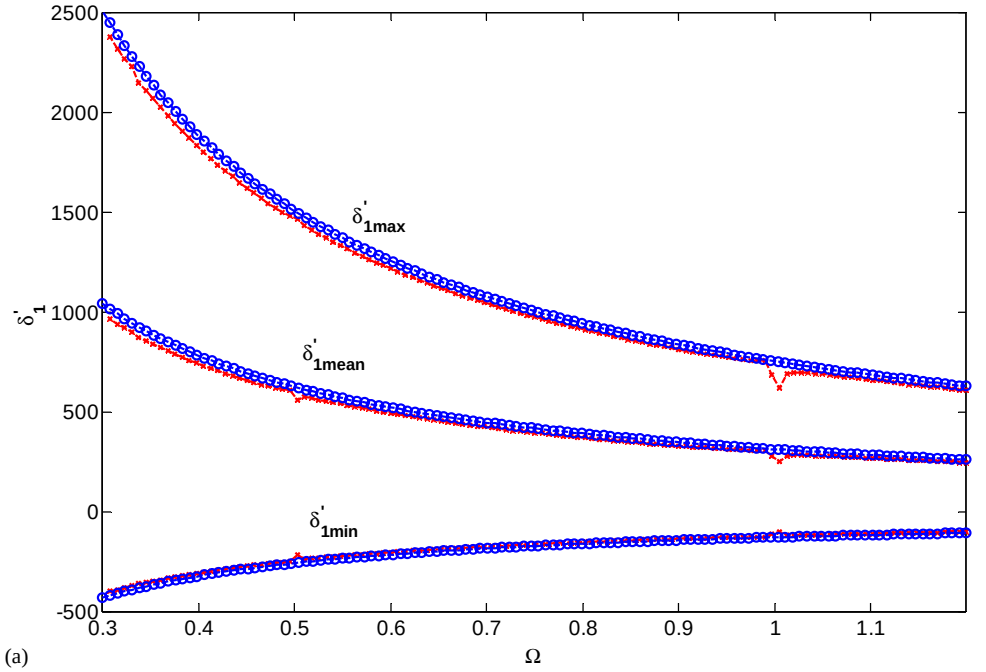

(a)

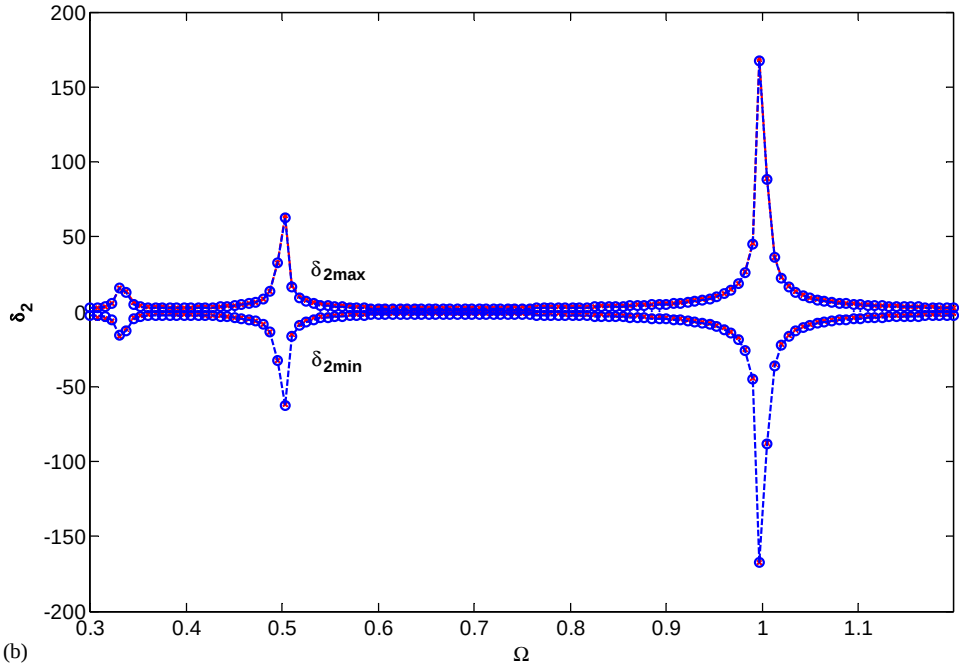

(b)

Fig. 7. Frequency responses for system of Fig. 4. Given $I_1 = 0.01$, $\zeta = 0.001$, $T_m = 0.5$, $T_p = 4.5$. (a) Max-mean-min frequency responses of δ_1': - -o- -, analytical solution; - -x- -, numerical solution. (b) Max–min frequency responses of δ_2: - -o- -, analytical solution; - -x- -, numerical solution.

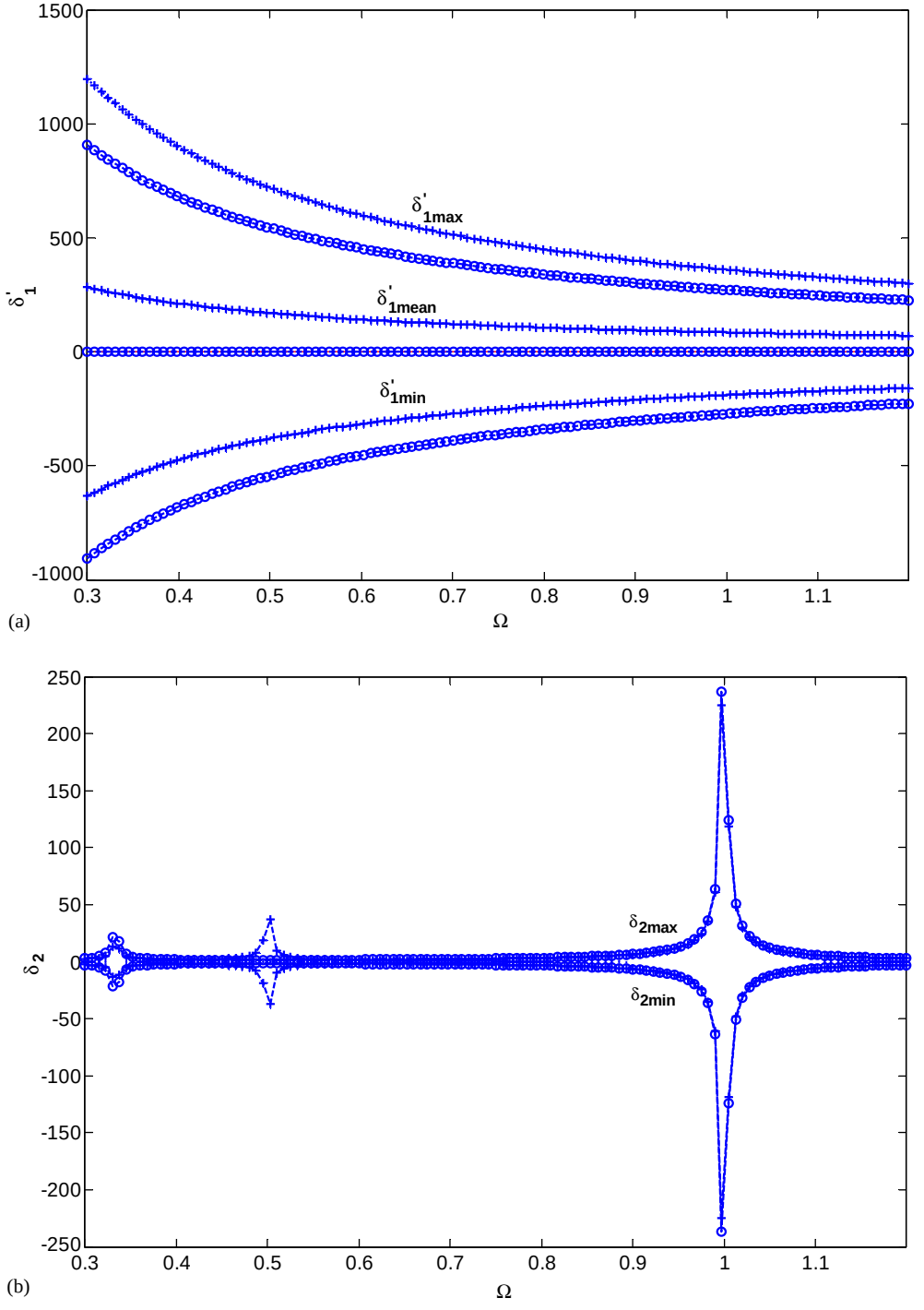

Fig. 8. Frequency responses for system of Fig. 4. Given $I_1 = 0.01$, $\zeta = 0.001$, $T_p = 4.5$. (a) Max-mean-min responses of δ_1': - -o- -, $T_m = 0$; - -+- -, $T_m = 0.2$. (b) Max–min responses of δ_2: - -o- -, $T_m = 0$; - -+- -, $T_m = 0.2$.

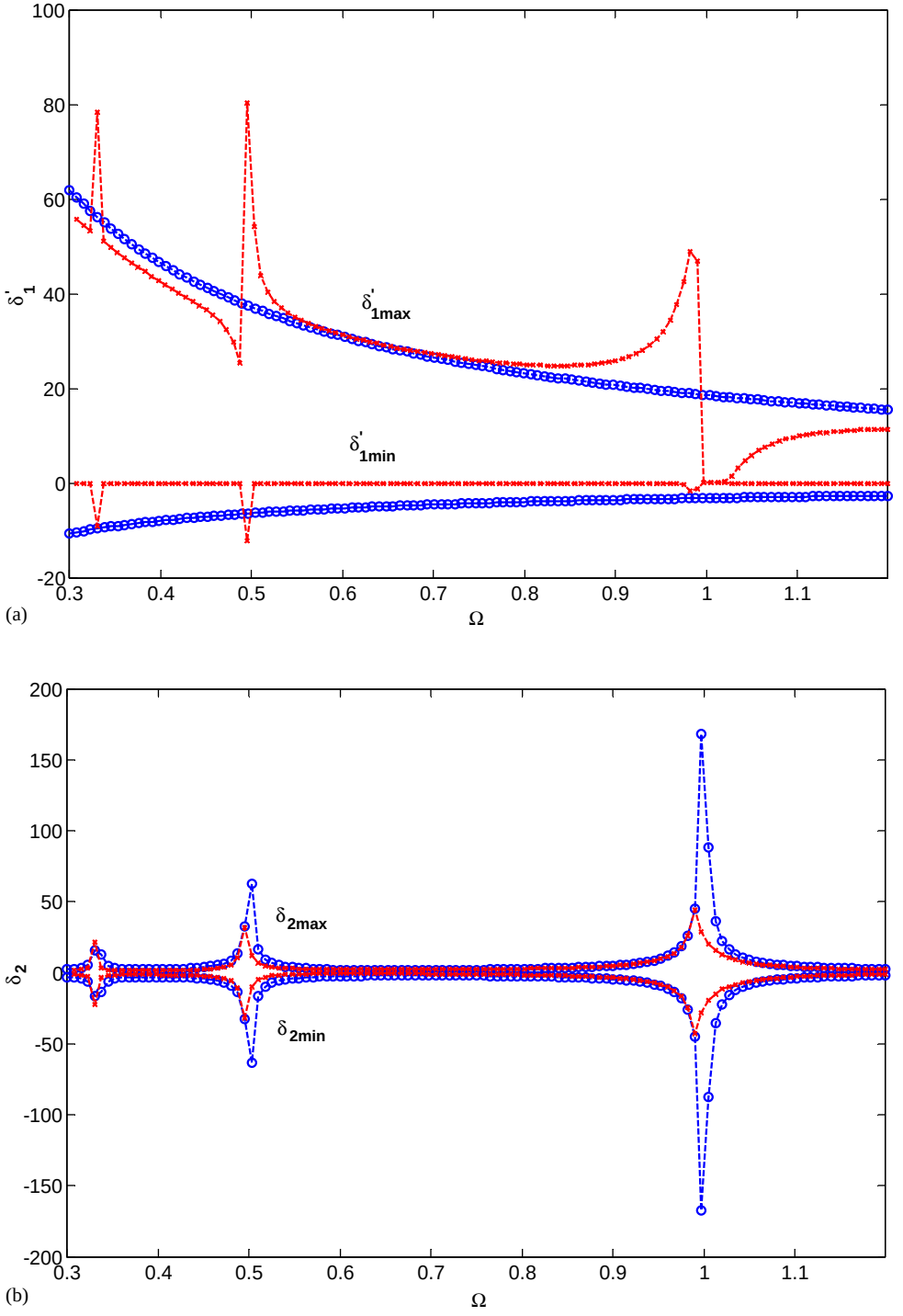

Fig. 9. Frequency responses for system of Fig. 4. Given $I_1 = 0.04$, $\zeta = 0.001$, $T_m = 0.5$, $T_p = 1.0$. (a) Max–min frequency responses of δ_1': - -o- -, analytical solution; - -x- -, numerical solution. (b) Max–min frequency responses of δ_2: - -o- -, analytical solution; - -x- -,numerical solution.

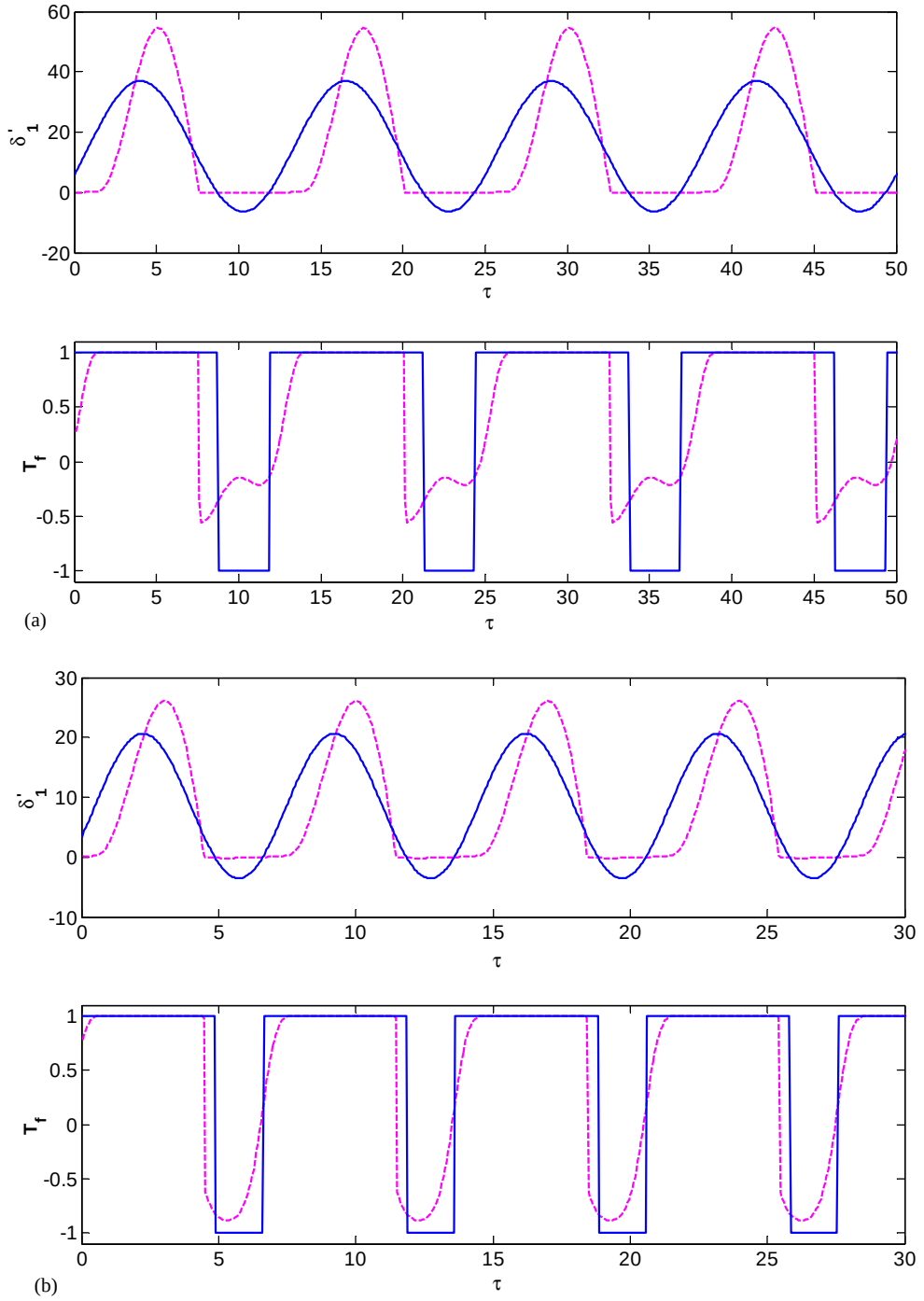

Fig. 10. Time histories for system of Fig. 4. Given $I_1 = 0.04$, $\zeta = 0.001$, $T_m = 0.5$, $T_p = 1.0$. (a) δ_1' and T_f at $\Omega = 0.5$: —, analytical solution; - - -, numerical solution. (b) δ_1' and T_f at $\Omega = 0.9$: —, analytical solution; - - -, numerical solution.

5. Refined MHBM

5.1. Formulation

Consider the torsional system of Fig. 1(a) again and observe that no spring element exists in parallel with the dry friction element. Consequently, the relative displacement $\delta_1(\tau)$ would grow monotonically with a mean velocity and thus it cannot be defined as a periodic function under the effect of T_m. Instead, the relative velocity $\delta_1'(\tau)$ is assumed to be periodic and is expressed as a truncated Fourier series as

$$\delta_1'(\tau) = a_o + \sum_{n=1}^{nh} a_{2n-1}\,\sin(n\Omega\tau) + a_{2n}\,\cos(n\Omega\tau). \tag{19a}$$

Similarly, the relative displacement $\delta_2(\tau)$ and the nonlinear friction torque $f(\delta_1')$ are expanded in the form of Fourier series:

$$\delta_2(\tau) = b_o + \sum_{n=1}^{nh} b_{2n-1}\,\sin(n\Omega\tau) + b_{2n}\,\cos(n\Omega\tau), \tag{19b}$$

$$f(\delta_1') = c_o + \sum_{n=1}^{nh} c_{2n-1}\,\sin(n\Omega\tau) + c_{2n}\,\cos(n\Omega\tau). \tag{19c}$$

First, substitute Eqs. (19b) and (19c) into Eq. (7b) and sort out the like terms on both sides to yield

$$b_o = c_o, \quad b_{2n-1}(1-n^2\Omega^2) - b_{2n}2\zeta_2 n\Omega = c_{2n-1}, \tag{20a,b}$$

$$b_{2n-1}2\zeta_2 n\Omega + b_{2n}(1-n^2\Omega^2) = c_{2n}. \tag{20c}$$

Represent the above in matrix form to yield the following where $\underline{\underline{H}}$ is a characteristic matrix of the linear sub-system of Fig. 4(b):

$$\underline{\underline{H}}\,\underline{b} = \underline{c}, \quad \underline{b} = \underline{\underline{H}}^{-1}\,\underline{c}, \tag{21a,b}$$

$$\underline{b} = \begin{pmatrix} b_o & b_1 & b_2 & \cdots & b_{2nh} \end{pmatrix}^{\mathrm{T}}, \quad \underline{c} = \begin{pmatrix} c_0 & c_1 & c_2 & \cdots & c_{2nh} \end{pmatrix}^{\mathrm{T}}, \tag{21c,d}$$

$$\underline{\underline{H}} = \begin{bmatrix} 1 & & & & \\ & \ddots & & & \\ & & \begin{bmatrix} 1-n^2\Omega^2 & -2\zeta n\Omega \\ 2\zeta n\Omega & 1-n^2\Omega^2 \end{bmatrix} & & \\ & & & & \ddots \end{bmatrix}. \tag{21e}$$

The introduction of $\underline{\underline{H}}$ would efficiently reduce the original 2dof system problem into a sdof system problem. Further, the characteristic matrix concept can be extended to a linear sub-system

of very large dimension, thus allowing a nonlinear path synthesis concept similar to Rook's formulation [17].

The time domain response $\delta_1'(\tau)$ can be written in terms of a discrete vector δ_1' by utilizing a discrete Fourier transform (DFT) matrix $\underline{\underline{\Delta}}$ where $\underline{a}$ is the corresponding Fourier coefficients of $\delta_1'(\tau)$ [18]. Generally, the number of discrete points to represent a steady-state response cycle is a multiple of 2, i.e. $N = 2^p$. This is consistent with the requirement of a fast Fourier transform routine:

$$\underline{\delta_1'}(\tau) = \begin{pmatrix} \delta_1'(\tau_o) & \delta_1'(\tau_1) & \cdots & \delta_1'(\tau_{N-1}) \end{pmatrix}^{\mathrm{T}} = \underline{\underline{\Delta}}\,\underline{a}. \tag{22a}$$

Similarly:

$$\underline{\delta_2}(\tau) = \underline{\underline{\Delta}}\,\underline{b}. \tag{22b}$$

Introduce a differential operator $\underline{\underline{D}}$ as

$$\underline{\underline{D}} = \begin{bmatrix} 0 & & & & \\ & \ddots & & & \\ & & \begin{bmatrix} 0 & -n \\ n & 0 \end{bmatrix} & & \\ & & & \ddots & \end{bmatrix}. \tag{23}$$

Thus, we have

$$\underline{\delta_1'}(\tau) = \Omega\,\underline{\underline{\Delta}}\,\underline{\underline{D}}\,\underline{a}, \quad \underline{\delta_2'}(\tau) = \Omega\,\underline{\underline{\Delta}}\,\underline{\underline{D}}\,\underline{b}, \quad \underline{\delta_2''}(\tau) = \Omega^2\,\underline{\underline{\Delta}}\,\underline{\underline{D}}^2\,\underline{b}. \tag{24a–c}$$

The nonlinear torque is also written as $\underline{f}(\delta_1') = \underline{\underline{\Delta}}\,\underline{c}$, which implies $\underline{c} = \underline{\underline{\Delta}}^+\underline{f}$ where $\underline{\underline{\Delta}}^+ = (\underline{\underline{\Delta}}^{\mathrm{T}}\,\underline{\underline{\Delta}})^{-1}\underline{\underline{\Delta}}^T$. The torque excitation is also defined in the form $\underline{T_e}(\tau) = \underline{\underline{\Delta}}\,\underline{Q}$, where $\underline{Q}$ is a known vector. Substitute Eqs. (19)–(24) into Eq. (4) and define the residue $\underline{\underline{\Delta}}\,\underline{R}$ in the time domain as

$$\underline{\underline{\Delta}}\,\underline{R} = I_1\Omega\,\underline{\underline{\Delta}}\,\underline{\underline{D}}\,\underline{a} + I_1\Omega^2\,\underline{\underline{\Delta}}\,\underline{\underline{D}}^2\,\underline{b} + \underline{\underline{\Delta}}\,\underline{c} - \underline{\underline{\Delta}}\,\underline{Q}. \tag{25}$$

Further, substituting $\underline{b} = \underline{\underline{H}}^{-1}\,\underline{c} = \underline{\underline{H}}^{-1}\underline{\underline{\Delta}}^+\underline{f}$ and pre-multiplying both sides by $\underline{\underline{\Delta}}^+$, the residue in the frequency domain ($\underline{R}$) is obtained:

$$\underline{R} = I_1\Omega\,\underline{\underline{D}}\,\underline{a} + \left[I_1\Omega^2\underline{\underline{D}}^2\underline{\underline{H}}^{-1}\underline{\underline{\Delta}}^+ + \underline{\underline{\Delta}}^+\right]\underline{f} - \underline{Q}. \tag{26}$$

Essentially, our MHBM minimizes $\underline{R}$ in the frequency domain by using an iterative approach. For instance, the Newton–Raphson iteration has been widely used [14,17,18]. In this process, a Jacobian Matrix $\underline{\underline{J}}$ is first defined as

$$\underline{\underline{J}} = \frac{\partial\,\underline{R}}{\partial\,\underline{a}} = I_1\Omega\,\underline{\underline{D}} + \text{'}\left[I_1\Omega^2\underline{\underline{D}}^2\underline{\underline{H}}^{-1}\underline{\underline{\Delta}}^+ + \underline{\underline{\Delta}}^+\right]\frac{\partial\,\underline{f}}{\partial\,\underline{a}}. \tag{27}$$

Here, $\partial\,\underline{f}\,/\partial\,\underline{a}$ can be calculated by the chain rule as

$$\frac{\partial\,\underline{f}}{\partial\,\underline{a}} = \frac{\partial\,\underline{f}}{\partial\,\underline{\delta_1'}}\frac{\partial\,\underline{\delta_1'}}{\partial\,\underline{a}} = \frac{\partial\,\underline{f}}{\partial\,\underline{\delta_1'}}\underline{\underline{\Delta}}. \tag{28}$$

At each iterative step, the value of $\underline{a}$ is updated as

$$\underline{a_{k+1}} = \underline{a_k} - \underline{\underline{J_k^{-1}}}\,\underline{R_k}. \tag{29}$$

5.2. Computational issues and choice of initial conditions

The following error criteria are usually followed [5,14,18,21] where ε is a pre-defined numerical tolerance:

$$\|a_{k+1} - a_k\| \leqslant \varepsilon, \quad \|R_{k+1} - R_k\| \leqslant \varepsilon. \tag{30a,b}$$

Here, $\|\|$ represents the Euclidean or L_2 norm. When the Jacobian matrix is ill-conditioned, the first criterion (30a) is more reliable [19]. The chief benefit of the Newton–Raphson technique is its quadratic convergence feature, i.e. $\|R_{k+1} - R_k\| = \mathrm{O}\|R_k - R_{k-1}\|^2$, where O represents order of magnitude. To take advantage of the quick convergence ability, the partial derivative of the residue has to be evaluated as in Eq. (27). This implies the nonlinear function has to be continuous as indicated in Eq. (28). This is however not the case for the classical Coulomb friction formulation in which a discontinuity exists at zero velocity. Therefore, a smoothening or conditioning procedure, using the hyperbolic or arctangent function, has been usually employed by some researchers [11,18,20,21]. In our study, a hyperbolic tangent function is used to approximate the classic Coulomb friction function:

$$T_f = f(\delta_1') \simeq \tanh(\sigma\delta_1'), \quad \frac{\partial f}{\partial \delta_1'} = \sigma[1 - \tanh^2(\sigma\delta_1')]. \tag{31a,b}$$

Duan and Singh [11] have shown that the conditioning factor σ should be very carefully chosen to ensure an appropriate representation of the theoretical discontinuous Coulomb friction when a direct Runge–Kutta fourth (fifth) numerical integration scheme is employed. Kim et al. [21] discussed the effect of the "smoothening factor" on nonlinear frequency responses with application of clearance type nonlinearity. Our harmonic balance method is also sensitive to the choice of σ. The chief reason lies in the calculation of $\partial \underline{f}/\partial\,\underline{\delta_1'}$ that plays an important role in the Jacobian matrix:

$$\frac{\partial \underline{f}}{\partial\,\underline{\delta_1'}} = \mathrm{diag}\left[\left.\frac{\partial f}{\partial \delta_1'}\right|_{\tau=\tau_0} \left.\frac{\partial f}{\partial \delta_1'}\right|_{\tau=\tau_1} \cdots \left.\frac{\partial f}{\partial \delta_1'}\right|_{\tau=\tau_{N-1}}\right]. \tag{32}$$

As evident from Eq. (31a), a lower value of σ would make the stick to slip transition more smooth and thus it is desirable in terms of numerical convergence. However, a more smooth transition would indicate fewer harmonics are contained in the approximated friction torque as explained by the Gibbs phenomena. Consequently, the calculated response may not be sufficiently accurate especially when the super-harmonic components significantly contribute to the overall response. On the other hand, a high value of σ is intuitively preferred. Mathematically, as the value of σ increases, the approximated $T_f = f(\delta_1')$ asymptotically converges to the discontinuous Coulomb friction. However, the values of $\partial f/\partial\delta_1'$ vary from relatively large numbers (corresponding to the stick state) to almost zeros (corresponding to the slip state) as obtained by Eq. (31b). The order of magnitude difference in such numerical values would ultimately contribute to the numerical

stiffness of the Jacobian matrix that could be defined by the ratio of the largest to the smallest non-zero local eigenvalues [22]. The widely separated eigenvalues in turn would indicate the coexistence of slowly varying and rapidly varying responses when the solution is slightly perturbed. This would require unreasonably small calculation steps to warrant numerical stability. Thus it would hinder convergence especially when significant stick–slip motions take place. We selected $\sigma = \mathrm{O}(50)$ when 256 discrete points are used to represent the continuous time history within an excitation cycle. The resulting responses have been validated by using a discontinuous numerical integration scheme that is already documented in an earlier study [11].

Further, the initial guess of solution $\underline{a_0}$ is very important for the predictor-corrector type exercises [23]. If $\underline{a_0}$ is far away from true solution, the convergence speed of Newton–Raphson is limited because the quadratic convergence seems to occur only during last steps. In the worst possible case, convergence may not be achieved at all and the solution could diverge. But much of the previous work on this topic [4,5,14,18] does not address this issue in sufficient detail. One approach is to just make a random guess [18]. Further, Wang and Chen [5] have proposed that one could use the first-order (one-term) harmonic balance solution as the initial guess for a bi-linear hysteresis problem. But as seen in Fig. 9, our one-term harmonic balance solution is still sufficiently far from the true solution. Consequently, we propose the following scheme. First, determine the stick-to-slip boundaries prior to a nonlinear analysis, using a similar procedure introduced by Duan and Singh [11]. For the sake of clarity, this procedure is briefly introduced here. When the frictional element is under the pure stick condition, $\bar{I}_1$ and $\bar{I}_2$ stick together to form a single rigid body and the system in Fig. 1(a) degenerates into a sdof system. Consequently, the governing equation, in the dimensionless form, is as

$$(I_1 + 1)\delta'' + 2\zeta\delta' + \delta = T_m + T_p \sin(\Omega\tau). \tag{33}$$

The corresponding steady-state forced harmonic response is

$$\delta(\tau) = T_m + \frac{T_p}{\sqrt{(1 - (I_1 + 1)\Omega^2)^2 + (2\zeta\Omega)^2}} \sin(\Omega\tau + \varphi), \tag{34a}$$

$$\varphi = -\tan^{-1} \frac{2\zeta\Omega}{1 - (I_1 + 1)\Omega^2}. \tag{34b}$$

Under the pure stick condition, the frictional torque in the interface is the difference between the excitation torque and the inertial torque $I_1\delta''$, where $\delta'' = -\Omega^2\delta$ is obtained from Eq. (34a):

$$T_f(\tau) = [T_m + T_p \sin(\Omega\tau)] - [I_1(-\Omega^2\delta(\tau))], \tag{35}$$

$$T_f(\tau) = T_m + T_p \sin(\Omega\tau) + I_1 \frac{T_p\Omega^2}{\sqrt{(1 - (I_1 + 1)\Omega^2)^2 + (2\zeta\Omega)^2}} \sin(\Omega\tau + \varphi). \tag{36}$$

Thus, the criterion to determine the stick-to-slip transition is defined as follows where $|\,|$ represents the absolute value:

$$|T_f| > T_{\mathrm{sf}}. \tag{37}$$

Using this criterion, the frequency regime(s) over which the pure stick condition takes place can be found by numerically sweeping the excitation frequency in either downward or upward direction. Additionally, the determination of stick-to-slip boundaries would not only bound the frequency regime over which the nonlinear analysis is needed, but it could also provide a good clue regarding the initial frequency for a sweep up or down; Note that the zeros are natural choices in the initial guess of $\underline{a_0}$. This way, the solution at the initial frequency is easily obtained. Given a high-frequency resolution, the response at subsequent frequencies can be conveniently determined by assuming the solution at the previous frequency as the initial guess.

6. Nonlinear responses and super-harmonics

6.1. Typical nonlinear responses and effect of mean load

Table 1 lists typical parameters (in the dimensionless form) of an automotive driveline system. As noted before, the saturated dry friction torque is generally high for a realistic TCC, in contrast with the dry frictional damper system, for the following reasons: to increase the fuel efficiency by allowing more power transmitted to the downstream system and to avoid thermal issues induced by excessive slipping motions [7,24]. For example, the friction torque capacity of a typical dry friction torque converter clutch is typically of the same order of magnitude as the peak dynamic torque generated by a nominal multi-cylinder engine [24,25]. Further, unlike the simplified system that was studied in Section 3, I_1 representing flywheel, front cover and impeller is much higher than I_2 of the friction shoe assembly. Nonetheless, Duan and Singh [11] have shown that I_2 can still significantly affect the system dynamics.

The appearance of super-harmonic peaks is obviously related to the number of harmonics (n) that must be included by the MHBM. In our study, 12 harmonics are used to construct the stick–slip motions and accordingly, 12 terms are included in $\delta_2(t)$ as these should be enough to predict real-life periodic motions. Also, as more harmonics are included, the super-harmonic resonances like 1/12, 1/13 and 1/14, etc. will be squeezed into a smaller frequency region and this would pose some difficulty in distinguishing them. Thus, in our study, we will only show the frequency range starting from $\Omega = 0.12$ and assume a minimal coupling effect between the

Table 1
Parameters (in the dimensionless form) used to study an automotive driveline system corresponding to Fig. 1(a)

Parameter	Dimensionless value
I_1	10–20
I_2	1.0
ζ	0.02
K	1.0
T_{sf}	1.0
T_m	0–0.8
T_p	0.5–2.0

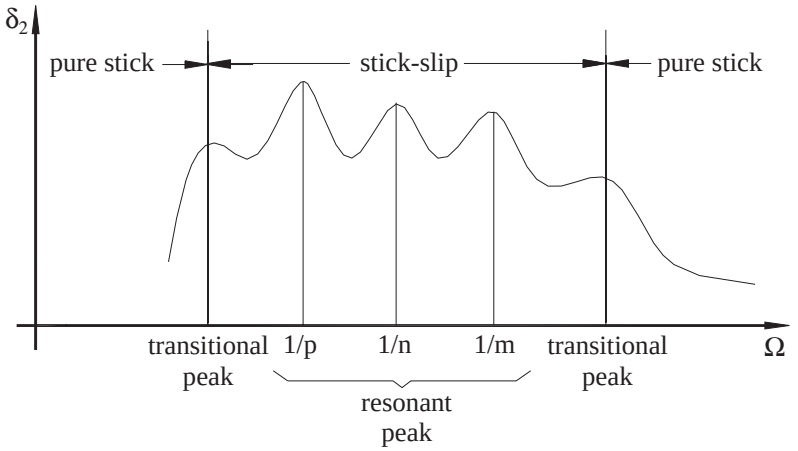

Fig. 11. A generic nonlinear frequency response map of δ_2 under significant stick–slip motions.

super-harmonics below $\Omega = 0.12$. Under the condition of significant stick–slip, a generic nonlinear frequency response map of δ_2 is illustrated in Fig. 11. As shown, two types of peaks could be present. The first type is the transitional peak which occurs as the frictional interface undergoes sudden transition from a pure stick state to the stick–slip state. The second type is the resonant peak which occurs at $\Omega \simeq 1/n$ due to the system resonance effect.

Fig. 12 represents a typical nonlinear frequency response when significant stick–slip motions occur. Fig. 13 shows a sample time history at $\Omega = 0.23$. The semi-analytical solutions match quite well with numerical solutions. The difference in the $T_f(\tau)$ plot of Fig. 13(c) clearly illustrates the Gibbs phenomena. Further, super-harmonic peaks in Fig. 12(b) can be seen at $\Omega \simeq 1/3, 1/4, 1/5, 1/7$, etc. However, it should be noted that the peak response at $\Omega = 1/2$ cannot be presumed to be a super-harmonic peak. In fact, it is a transitional peak, as evident from Fig. 12(a). When the system parameters and excitation change, the transition frequency will also change. This transition frequency can be determined by the procedure introduced in Section 5.2, ahead of the nonlinear calculation. Again, the calculated nonlinear frequency response of δ_2 is much different from the anticipated linear system response for which a primary harmonic resonance occurs at $\Omega \simeq 1.0$ as in Fig. 3(b). Instead, the super-harmonic peaks dominate the response level at low frequencies and the primary harmonic resonance is not excited at all. Further, it is noted that three harmonic terms are not sufficient to represent significant stick–slip motions as shown in Fig. 12.

Again, the effect of T_m is investigated. Fig. 14 presents the nonlinear frequency responses for $T_m = 0$. Compare these with Fig. 12 and observe that the existence of non-zero T_m has an effect on the frequency responses similar to the one discussed in Section 4 for a simplified system. When $T_m = 0$, symmetric stick–slip motions are strictly followed as seen in Fig. 14(a). But asymmetric stick–slip motions take place at $T_m = 0.5$ as observed in Fig. 12(a). Further, more super-harmonic peaks are excited by the friction torque that is generated by the asymmetric stick–slip. For example in Fig. 14, when $T_m = 0$, super-harmonic resonances only occur around $\Omega \simeq 1/4$ and $1/6$; but when $T_m = 0.5$, resonances take place around $\Omega \simeq 1/3, 1/4, 1/5, 1/7$, etc. as shown

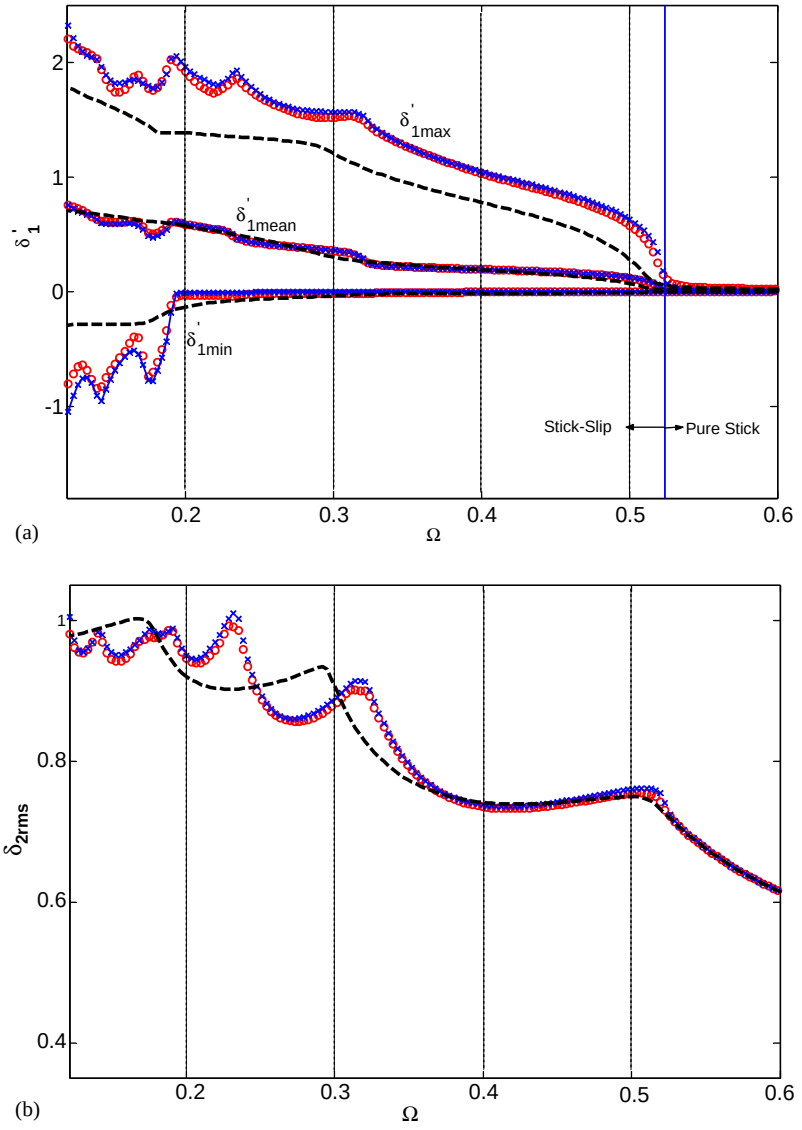

Fig. 12. Frequency response for system of Fig. 1(a). Given $I_1 = 10$, $\zeta = 0.02$, $T_m = 0.5$, $T_p = 1.5$. (a) Max–min frequency responses of δ_1': ooo, semi-analytical solution with 12 harmonic terms; - - -, semi-analytical solution with three harmonic terms; xxx, numerical solution. (b) rms frequency response of δ_2: ooo, semi-analytical solution with 12 harmonic terms; - - -, semi-analytical solution with three harmonic terms; xxx, numerical solution.

in Fig. 12(b). However, under significant stick–slip motions, the generated friction torque as in Fig. 13 is no longer a pulse excitation as in Figs. 6 and 10. It is hard to analytically predict which super-harmonic peaks will appear unlike the simple case studied in Section 4. Nevertheless, semi-analytical methods such as MHBM or numerical integration can be utilized to find the resonant peaks.

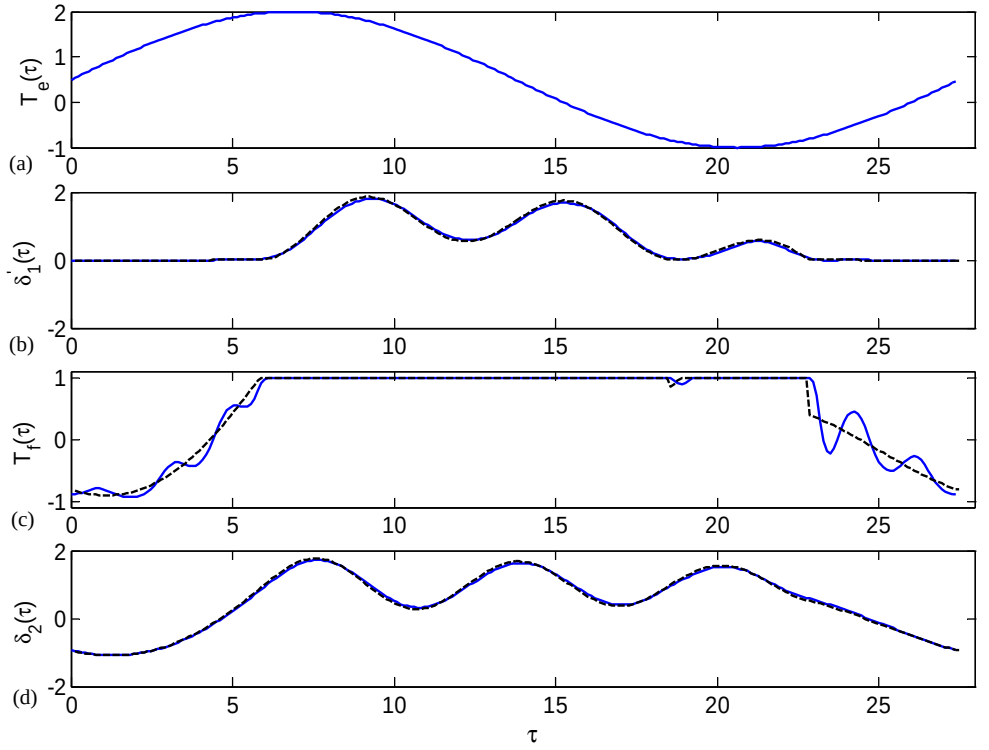

Fig. 13. Time histories at $\Omega = 0.23$ for system of Fig. 1(a). Given $I_1 = 10$, $\zeta = 0.02$, $T_m = 0.5$, $T_p = 1.5$. (a) Harmonic excitation torque. (b) Time history of δ_1': —, semi-analytical solution;- - -, numerical solution. (c) Time history of T_f: —, semi-analytical solution; - - -, numerical solution. (d) Time history of δ_2: —, semi-analytical solution; - - - , numerical solution.

6.2. *Effect of the number of harmonics on resonant peaks*

As discussed in Section 4, the super-harmonic contents in $T_f(\tau)$ induced by pure slip or stick–slip motions will generate super-harmonic response in $\delta_2(\tau)$. Accordingly, resonant peaks at lower Ω as in Figs. 12(b) and 14(b) occur. However, in the case of significant stick–slip motions, it does not mean the nth super-harmonic component of δ_2 would always dominate the time history when excited at $\Omega \simeq 1/n$. For instance, consider the time history corresponding to the peak around $\Omega = 0.32$ (1/3 super-harmonic peak) as shown in Fig. 15(a). The response is dictated by the first four harmonics and the mean ($n = 0$) part. At the peak around $\Omega \simeq 0.23$ (1/4 super-harmonic peak) in Fig. 15(b), the response is dictated by the first five harmonics and the mean part. The dominance of the $n = 1$ and 2 components is due to the sticking phase which prevails in the stick–slip response. The difference in rms value responses as shown in Fig. 12(b) is due to the involvement of more period-motions (or more harmonics) in the time history.

The mechanism of generating super-harmonic peaks discussed above can be further explained by a 3-D response map that is constructed in Fig. 16. The x coordinate indicates the harmonic order n (including the dc part) of the response of δ_2; the y coordinate is the excitation frequency Ω

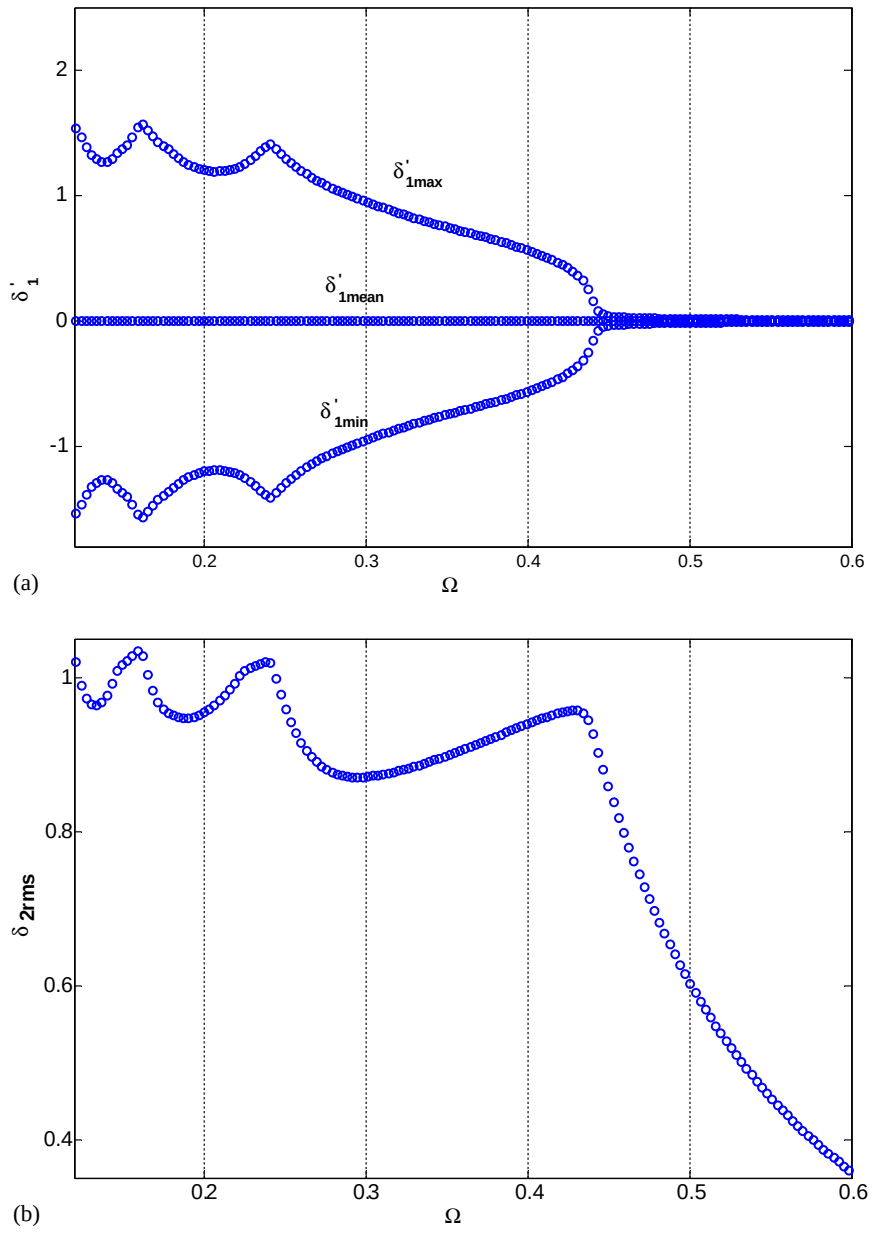

Fig. 14. Frequency responses for system of Fig. 1(a). Given. $I_1 = 10$, $\zeta = 0.02$, $T_m = 0$, $T_p = 1.0$. (a) Max–min frequency responses of δ_1', (b) rms frequency response of δ_2.

and the z coordinate is the response amplitude δ_2. As seen in Fig. 16, $n = 0, 1$ and 2 components contribute much to the overall response over the entire frequency regime, which is consistent with our observation at $\Omega \simeq 0.32$ and 0.23. As Ω moves down, more super-harmonic components get involved. Accordingly, various resonant peaks are formulated.

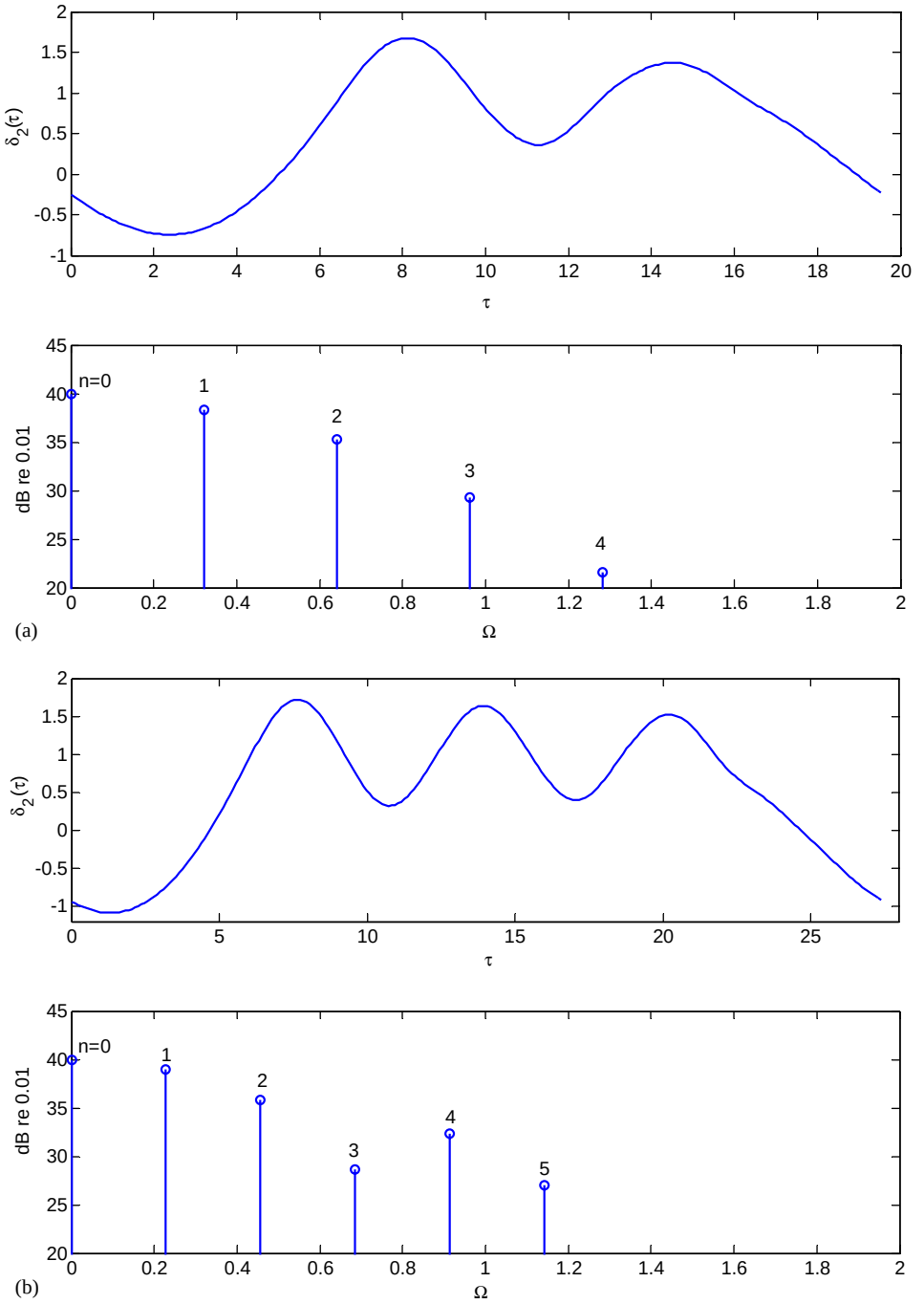

Fig. 15. Time histories and Fast Fourier Transform of δ_2. Given $I_1 = 10$, $\zeta = 0.02$, $T_m = 0.5$, $T_p = 1.5$. (a) $\Omega = 0.32$, (b) $\Omega = 0.23$.

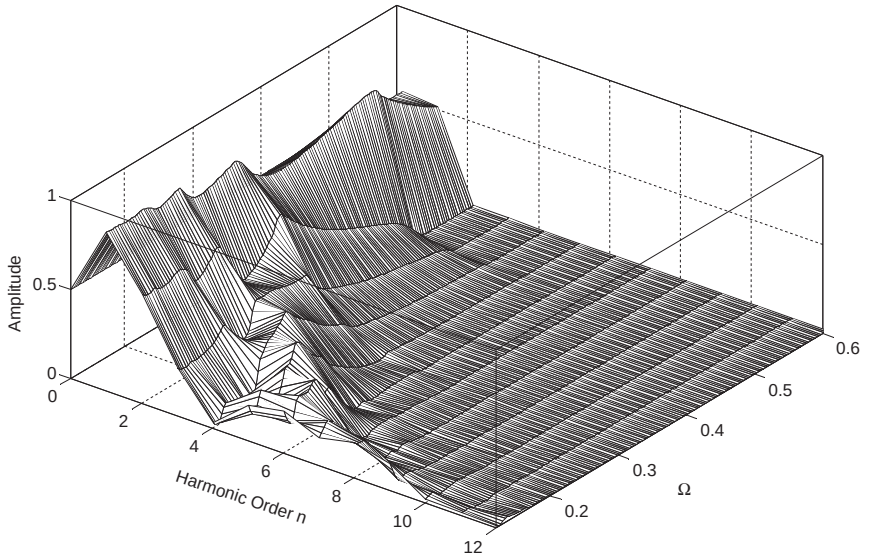

Fig. 16. 3-D response map for system of Fig. 1(a). Given $I_1 = 10,\ \zeta = 0.02,\ T_m = 0.5,\ T_p = 1.5$.

7. Effect of negative slope in friction formulation

Finally, we study a more general friction formulation, with different static (μ_s) and kinetic (μ_k) friction coefficients. In the following formulation [26], μ_k has been normalized with respect to $\mu_s(= 1.0)$, α is a factor that controls the exponentially decaying gradient and sgn is the signum function.

$$T_f(\delta_1') = f(\delta_1') = \begin{cases} [\mu_k + (1.0 - \mu_k)\mathrm{e}^{-\alpha|\delta_1'|}]\,\mathrm{sgn}(\delta_1'), & |\delta_1'| > 0, \\ [0 \quad 1.0], & \delta_1' = 0, \end{cases} \tag{38}$$

$$\mathrm{sgn}(\delta_1') = \begin{cases} \frac{\delta_1'}{|\delta_1'|}, & |\delta_1'| > 0, \\ 0, & \delta_1' = 0. \end{cases} \tag{39}$$

We can further condition the discontinuous formulation (38) by a hyperbolic-tangent function.

$$f(\delta_1') = [\mu_k + (1.0 - \mu_k)\mathrm{e}^{-\alpha|\delta_1'|}]\tanh(\sigma\delta_1'), \tag{40a}$$

$$\frac{\partial f}{\partial \delta_1'} = \sigma[\mu_k + (1.0 - \mu_k)\mathrm{e}^{-\alpha|\delta_1'|}][1.0 - \tanh^2(\sigma\delta_1')] - \alpha(1.0 - \mu_k)\mathrm{e}^{-\alpha|\delta_1'|}\mathrm{sgn}(\delta_1')\tanh(\sigma\delta_1'). \tag{40b}$$

Note that when $\mu_k < 1.0$, a negative slope ($\partial f/\partial\delta_1' < 0$) is found in the friction law. Insert $f(\delta_1')$ and $\partial f/\partial\delta_1'$ into Eqs. (26) and (28) and apply the MHBM formulation of Section 5 with the provision that the system is still dynamically stable and the response is periodic. Consequently, only a minor variation in μ_k is permitted.

Fig. 17 compares the results for three values of μ_k (1.0, 0.95 and 0.9), given $\alpha = 2$. First, Fig. 17(a) shows that the stick-to-slip transition frequencies for all cases are almost identical as it should be since the friction capacity that is determined by μ_s (= 1.0) remains unchanged. Differences in δ_1' values are also seen at lower frequencies. As shown in Fig. 17(b), it appears that the downstream system response could be sensitive to μ_k. A minor change in μ_k here induces a relatively large difference in $\delta_{2\text{rms}}$, especially at the resonant frequencies. When μ_k is reduced, the

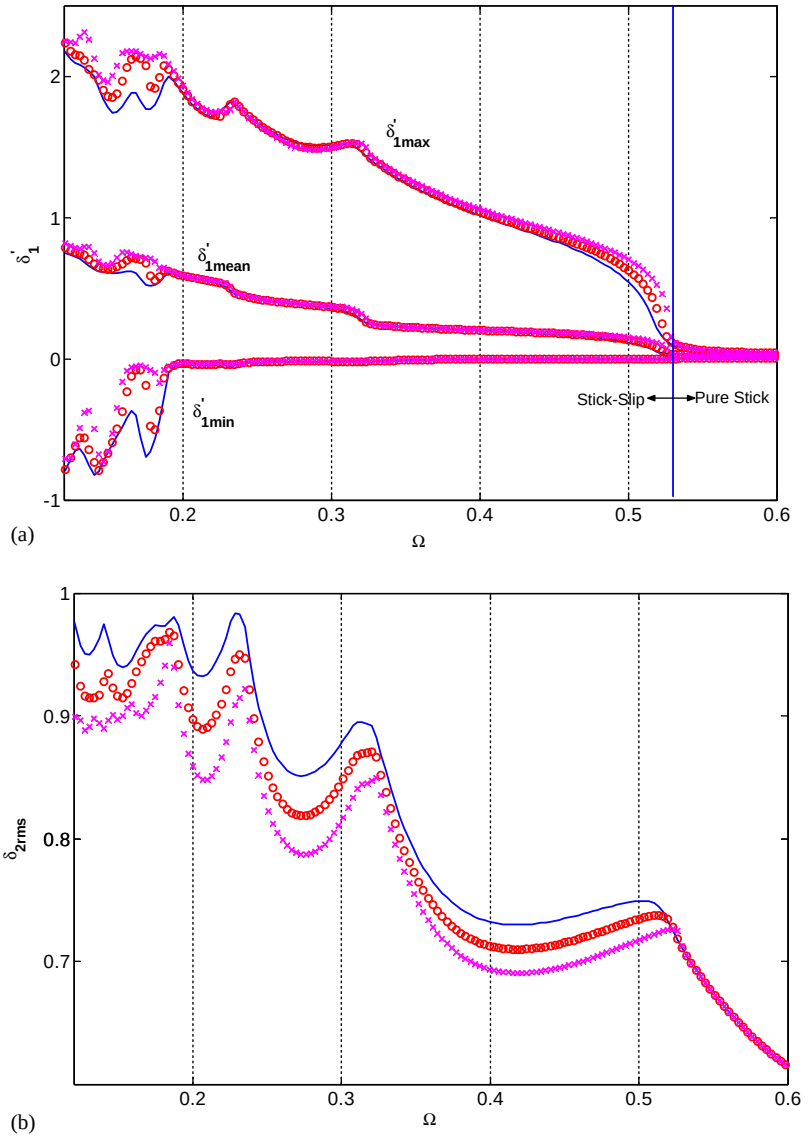

Fig. 17. Frequency response for system of Fig. 1(a). Given $I_1 = 10$, $\zeta = 0.02$, $T_m = 0.5$, $T_p = 1.5$. (a) Max–min frequency responses of δ_1': —, $\mu_k = 1.0$; ooo, $\mu_k = 0.95$; xxx, $\mu_k = 0.9$. (b) rms frequency response of δ_2: —, $\mu_k = 1.0$; ooo, $\mu_k = 0.95$; xxx, $\mu_k = 0.9$.

peak values of $\delta_{2\mathrm{rms}}$ are lower. This is because of the reduced friction torque during the slip state that is determined by the value of μ_k; this torque constitutes an equivalent excitation to the downstream sub-system. Similar to the variation in δ_1', the differences in $\delta_{2\mathrm{rms}}$ between three cases are more visible at lower frequencies where significant stick–slip motions tend to occur. Of course, a further decrease of μ_k will introduce numerical instabilities and chaotic responses. Those factors will pose difficulties on the application of MHBM that assumes periodic responses. A subsequent article will address this particular issue.

8. Comparison with conventional friction damper problem (Den Hartog's system)

Finally, we examine the conventional sdof friction damper system of Fig. 2 that has been studied by many researchers [1,2,14,20]. The governing equation is

$$\bar{I}_e\ddot{\bar{\delta}} + \bar{C}\dot{\bar{\delta}} + \bar{K}\bar{\delta} + \bar{T}_f(\dot{\bar{\delta}}) = \bar{T}_{me} + \bar{T}_{pe}\sin(\bar{\omega}\,\bar{t}), \qquad \bar{T}_f(\dot{\bar{\delta}}) = \bar{T}_{\mathrm{sf}}f(\dot{\bar{\delta}}). \tag{41a,b}$$

Again, it is non-dimensionalized by introducing the parameters

$$\omega_n = \sqrt{\frac{\bar{K}}{\bar{I}_e}}, \quad \zeta = \frac{\bar{C}}{2\sqrt{\bar{K}\bar{I}_e}}, \quad \delta = \frac{\bar{K}\bar{\delta}}{\bar{T}_{\mathrm{sf}}}, \tag{42a–c}$$

$$T_m = \frac{\bar{T}_{me}}{\bar{T}_{\mathrm{sf}}}, \quad T_p = \frac{\bar{T}_{pe}}{\bar{T}_{\mathrm{sf}}}, \tag{42d,e}$$

$$\Omega = \frac{\bar{\omega}}{\bar{\omega}_n}, \quad \tau = \frac{\bar{t}}{\bar{\omega}_n}. \tag{42f,g}$$

The following dimensionless governing equation is obtained where derivatives are with respect to τ:

$$\delta'' + 2\zeta\delta' + \delta + f(\delta') = T_m + T_p\sin(\Omega\tau). \tag{43}$$

First, note that T_m can be balanced out by the spring with a mean or static displacement $\langle\delta\rangle_\tau = T_m$. Thus the existence of non-zero T_m has no effect on the relative slip or stick–slip velocities. This is quite different from our 2dof system of Fig. 1(a). This implies the friction interface in Fig. 2 would always experience symmetric stick–slip motion, i.e. $\delta'(\tau) = -\delta'(\tau + P/2)$. Indeed, this was the basis of solution as originally proposed by Den Hartog [1]. Further, Eq. (41) can be simplified by excluding T_m and by re-setting $\delta(\tau)$:

$$\delta'' + 2\zeta\delta' + \delta + f(\delta') = T_p\sin(\Omega\tau). \tag{44}$$

Den Hartog developed the analytical solutions of Eq. (44) for two cases: pure slipping motion and two-stop motion. He also obtained a boundary (dashed line in Fig. 18) between the motions without any stop and with two stops. Based on Den Hartog's boundary, stick–slip motion tends to occur in the low-frequency range when the friction force or torque is generally high. This is consistent with our system of Fig. 1(a) as discussed in Section 6. Here, we employ the MHBM

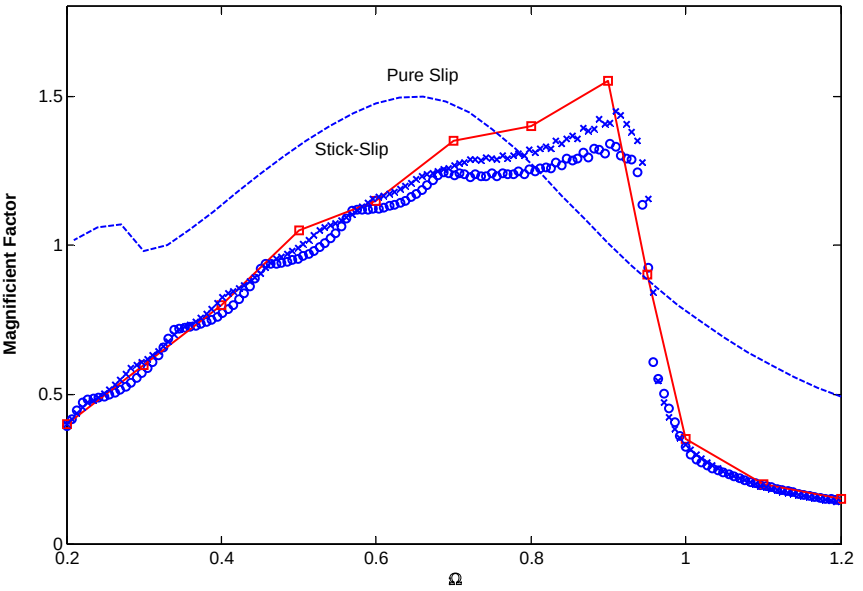

Fig. 18. Comparison between semi-analytical solution and Den Hartog's analytical solution. Given $\zeta = 0$ and $T_p = 1.25$ for system of Fig. 2. ooo, semi-analytical solution with 12 harmonics; xxx, semi-analytical solution with 24 harmonics; -□-, Den Hartog's analytical solution (from Fig. 4 of Ref. [1]).

(proposed in Section 5) to find the stick–slip responses. For the sake of brevity, only the case of $\zeta = 0$ and $T_p = 1.25$ is compared. Fig. 18 compares the calculated responses and Den Hartog's analytical solution. A good match is observed in terms of the magnification factors $(\delta_{0-\text{peak}}/(T_p/K))$ and peak frequency (f_{peak}). Minor differences are found around the f_{peak} regime. But these results could be improved by increasing n from 12 to 24. Further, as seen from the 3-D response map in Fig. 19, only the first harmonic dominates the response over the entire frequency regime. Although a third harmonic component is involved at lower Ω values, it is too weak to generate an active super-harmonic peak. This explains the absence of super-harmonic peaks in the sdof frequency responses, unlike the observations for the torsional system of Fig. 1(a) we studied in this article.

9. Conclusion

The nonlinear frequency response characteristics of a torsional system with dry friction controlled path have been studied. Three key contributions emerge. First, an analytical solution based on one-term harmonic balance is developed for a simplified torsional system subjected to continuous slipping motions. The nature of super-harmonic peaks as generated by the dry friction nonlinearity is efficiently found. The effect of a non-zero mean load is also determined and qualitatively understood. Second, a refined multi-term harmonic balance method (MHBM) is proposed to study an automotive drive train system that experiences significant stick–slip

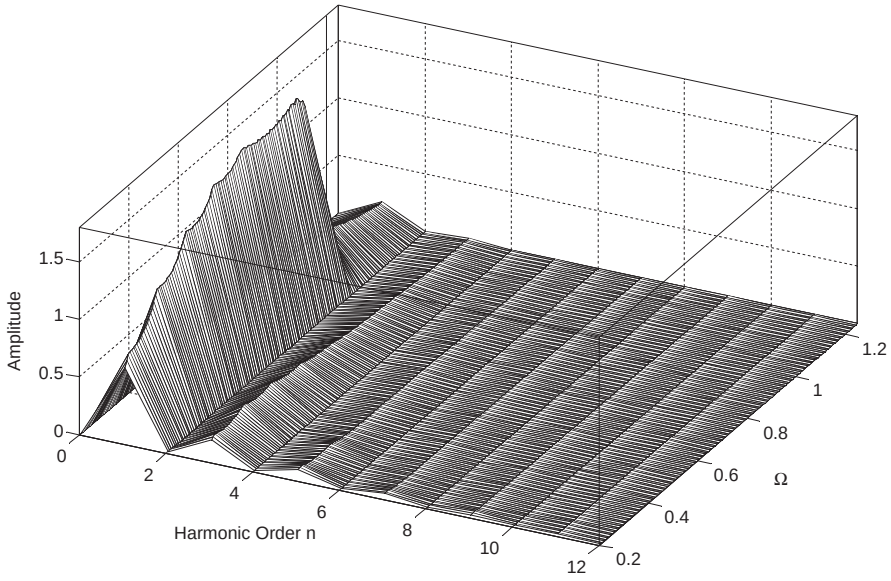

Fig. 19. 3-D response map for system in Fig. 2. Given $\zeta = 0$ and $T_p = 1.25$. Semi-analytical solutions used to construct this map.

motions. Our method includes up to 12 harmonics and yet yields responses in an efficient manner. Associated computational issues with the conditioning factor are addressed in detail. Moreover, a procedure to properly select the initial conditions is developed based on the linear system theory. Two types of peaks are seen in nonlinear frequency responses: transitional peaks and super-harmonic resonant peaks. The non-zero mean load in the mdof system has an effect similar to the simplified system and it generates asymmetric stick–slip motions. Further, studies have shown that the occurrence of super-harmonic resonant peaks is also related to the number of harmonic terms included in assumed solutions especially over the lower frequency regime. This is well explained by the 3-D response maps. Third, the conventional sdof dry friction damper system (Den Hartog's problem) in which a spring path is in parallel with a dry friction path is revisited. Our results show that this conventional system differs, in terms of the dynamic behavior, from our torsional system with a sole dry friction path (with a high saturation torque). In particular, the mean load in our system dictates the nature of nonlinear system responses. The sdof damper system response (Den Hartog's problem) is controlled by the primary harmonic resonance, unlike our torsional system (with a sole dry friction path) where many super-harmonic resonant peaks are present. Future work will deal with the periodic and transient response of the torsional system (with a dry friction path), as well as applications to real-life automotive problems.

Acknowledgements

Financial support through the DaimlerChrysler Challenge Fund is gratefully acknowledged.

References

[1] J.P. Den Hartog, Forced vibrations with combined Coulomb and viscous friction, *Transactions of the ASME* APM-53-9 (1931) 107–115.

[2] T.K. Pratt, R. Williams, Nonlinear analysis of stick/slip motion, *Journal of Sound and Vibration* 74 (4) (1981) 531–542.

[3] Y. Wang, An analytical solution for periodic response of elastic-friction damped systems, *Journal of Sound and Vibration* 189 (3) (1996) 299–313.

[4] C.H. Menq, B.D. Yang, Non-linear spring resistance and friction damping of frictional constraint having two-dimensional motion, *Journal of Sound and Vibration* 217 (1) (1998) 127–143.

[5] J.H. Wang, W.K. Chen, Investigation of the vibration of a blade with friction damper by HBM, *Transactions of the ASME, Journal of Engineering for Gas Turbines and Power* 115/295 (1993) 294–299.

[6] D. Karnopp, Computer simulation of stick–slip friction in mechanical dynamic systems, *Transactions of the ASME, Journal of Dynamic Systems, Measurement, and Control* 107 (1985) 100–103.

[7] R. Fischer, D. Otto, Torque converter clutch systems, *The Fifth Luk Symposium*, May 1994, pp. 107–138.

[8] A. Albers, Torque control isolation (TCI) the smart clutch, *Fourth International Luk Symposium*, Baden-Baden, April 20, 1990, pp. 81–107.

[9] R. Berger, R. Meinhard, B. Carsten, The parallel shift gearbox PSG, twin clutch gearbox with dry clutches, *Luk Symposium*, 2002, pp. 197–210.

[10] M. Goetz, M.C. Levesley, D.A. Crolla, Dynamic modeling of a twin clutch transmission for controller design, *Proceedings of the Fifth International Conference on Modern Practice in Stress and Vibration Analysis*, Material Science Forum, vols. 440–441, 2003, pp. 253–260.

[11] C. Duan, Dynamic analysis of dry friction path in a torsional system, *Ph.D. Dissertation*, The Ohio State University, 2004.

[12] G. Lechner, H. Naunheimer, *Automotive Transmissions: Fundamentals, Selection, Design and Application*, Springer, Berlin, 1999.

[13] R. Singh, H. Xie, R.J. Comparin, Analysis of automotive neutral gear rattle, *Journal of Sound and Vibration* 131 (2) (1989) 177–196.

[14] C. Pierre, A.A. Ferri, E.H. Dowell, Multi-harmonic analysis of dry friction damped systems using an incremental harmonic balance method, *Transactions of the ASME, Journal of Applied Mechanics* 52 (1985) 958–964.

[15] E.O. Doebelin, *System Modeling and Response: Theoretical and Experimental Approaches*, 1980.

[16] J.R. Dormand, P.J. Prince, A family of embedded Runge–Kutta formulae, *Journal of Computational and Applied Mathematics* 6 (1) (1980) 19–26.

[17] T. Rook, Noise path synthesis with nonlinear joints, *Nonlinear Dynamics* 30 (3) (2002) 295–312.

[18] T.C. Kim, T.E. Rook, R. Singh, Super- and sub-harmonic response calculations for a torsional system with clearance non-linearity using the harmonic balance method, *Journal of Sound and Vibration* (2004), in press.

[19] S.J. Leon, *Linear Algebra with Applications*, Macmillan, New York, 1990.

[20] B.L. Van De Vrande, D.H. Van Campen, A. De Kraker, An approximate analysis of dry-friction-induced stick–slip vibration by a smoothing procedure, *Nonlinear Dynamics* 19 (1999) 157–169.

[21] T.C. Kim, T.E. Rook, R. Singh, Effect of smoothening functions on the frequency response of an oscillator with clearance non-linearity, *Journal of Sound and Vibration* 263 (2003) 665–678.

[22] R.C. Aiken, *Stiff Computation*, Oxford University Press, Oxford, 1985.

[23] C.E. Gerald, *Applied Numerical Analysis*, Addison-Wesley, Reading, MA, 1980.

[24] Personal discussion with DaimlerChrysler powertrain engineers in April 2002.

[25] T. Imamura, O. Sato, K. Sano, K. Tomioka, Development of shift control for a 5-speed AT using Matlab, *JATCO Technical Review* 3 (2002) 31–37.

[26] E.J. Berger, Friction modeling for dynamic system simulation, *Applied Mechanics Review* 55 (6) (2002) 535–577.